Article

Genome-wide screen of *Mycobacterium tuberculosis*-infected macrophages revealed GID/CTLH complex-mediated modulation of bacterial growth

Nelson V. Simwela[1], Luana Johnston [1], Paulina Pavinski Bitar[2], Eleni Jaecklein[3], Craig Altier[2], Christopher M. Sassetti[3] & David G. Russell [1] ✉

The eukaryotic Glucose Induced Degradation/C-Terminal to LisH (GID/CTLH) complex is a highly conserved E3 ubiquitin ligase involved in a broad range of biological processes. However, a role of this complex in host anti-microbial defenses has not been described. We exploited *Mycobacterium tuberculosis* (*Mtb*) induced cytotoxicity in macrophages in a FACS based CRISPR genetic screen to identify host determinants of intracellular *Mtb* growth restriction. Our screen identified 5 (*GID8*, *YPEL5*, *WDR26*, *UBE2H*, *MAEA*) of the 12 predicted members of the GID/CTLH complex as determinants of intracellular growth of both *Mtb* and *Salmonella* serovar Typhimurium. We show that the anti-microbial properties of the GID/CTLH complex knockout macrophages are mediated by enhanced GABAergic signaling, activated AMPK, increased autophagic flux and resistance to *Mtb* induced necrotic cell death. Meanwhile, *Mtb* isolated from GID/CTLH knockout macrophages are nutritionally starved and oxidatively stressed. Our study identifies the GID/CTLH complex activity as broadly suppressive of host anti-microbial responses against intracellular bacterial infections.

Mycobacterium tuberculosis (*Mtb*) is an intracellular pathogen that causes tuberculosis (TB), the leading cause of global mortality due to a single infectious disease[1]. At the onset of infection, *Mtb* is inhaled into the airways and phagocytosed by resident alveolar macrophages. This initial interaction triggers the recruitment of monocyte-derived macrophages, which gradually become the more abundant host macrophage population as the infection becomes more established. It is estimated that only 5–10% of *Mtb*-infected individuals will progress to active TB disease[1]. Whether the non-progressors remain latently infected, or progress to clear the infection is a subject of ongoing debate[2]. *Mtb* has evolved to survive and grow within the macrophage through the subversion of the anti-microbial properties of the

phagocyte. In brief, the bacterium blocks normal phagosomal acidification and phagosome/lysosome fusion[3–6]. Inside the macrophage, the bacterium also relies on access to host fatty acids and cholesterol to fuel its biosynthetic demands[7]. The outcome of this interplay is strongly influenced by both the macrophage lineages involved and the development of an acquired immune response. It is now known that lung macrophages comprise two separate lineages; tissue-resident alveolar macrophages that are fetal stem cell-derived and populate the lung during embryogenesis, and interstitial macrophages that are derived from blood monocytes and are recruited to the lung upon insult or infection[8,9]. While resident alveolar macrophages are more permissive to *Mtb* growth, recruited interstitial macrophages are

[1]Department of Microbiology and Immunology, College of Veterinary Medicine, Cornell University, Ithaca, NY, USA. [2]Department of Population Medicine and Diagnostic Sciences, Cornell University, Ithaca, NY, USA. [3]Department of Microbiology and Physiological Systems, UMass Chan Medical School, Worcester, MA, USA. ✉e-mail: dgr8@cornell.edu

innately more hostile to the intracellular bacteria[10]. Eventually, *Mtb* parasitization of the macrophage usually ends in the death of the infected phagocyte. However, the route to cell death also plays a major role in bacterial survival. If the infected macrophage undergoes apoptosis, *Mtb* will likely be killed, either in the apoptotic body or as a result of efferocytosis[11,12]. In contrast, macrophage death via necrosis supports *Mtb* growth and aids in bacterial spread[13,14]. One of the most significant determinants of *Mtb* fate inside macrophages is its ability to perforate the phagosome by an *ESX-1* type VII secretion system[15]. Phagosomal damage releases *Mtb* effectors into the host cytosol that suppress apoptosis and drive necrosis[13,16]. Through the action of *ESX-1*, *Mtb* also inhibits macrophage anti-microbial defenses such as autophagy and inflammasome-mediated production of interleukin-1β (IL-1β)[17,18].

The route to macrophage cell death is clearly important to *Mtb*'s success as a pathogen. Two groups have conducted genome-wide CRISPR/Cas9 screens targeting *Mtb*-induced macrophage cell death pathways. Zhang and colleagues screened RAW264.7 cells and identified multiple genes in the type 1 interferon signaling pathway that, when disrupted, conferred protection against *Mtb*-induced cell death[19]. Similarly, Lai et al.[20] performed a whole genome screen on THP1 cells infected with *M. bovis* BCG and also identified hits in the type 1 interferon pathway as having protective effects on infected cells. Both of these screens used the diminished death of infected cells to select for genes that, when deleted, provided the cells with some degree of protection. In this study, we used a similar CRISPR screening approach but emphasized a different selection pressure. We hypothesized that improved cell survival could also be a result of mutations that restrict bacterial growth with the potential to identify novel host pathways of bacterial control. We performed a genome-wide CRISPR/Cas9 screen on primary Hoxb8 conditionally immortalized murine bone marrow macrophages and identified the mammalian GID/CTLH complex as a strong determinant of intracellular growth of *Mtb* in macrophages. We show that knockout of individual components of the GID/CTLH complex is strongly restrictive to the intracellular growth of *Mtb* and *S.* Typhimurium. Mechanistically, knockout of the GID/CTLH complex promotes anti-microbial responses in macrophages through an enhanced autophagic response, increased metabolic resilience, and resistance to cell death. GID/CTLH knockout macrophages are also anti-inflammatory and, at the same time, restrict intracellular *Mtb* access to essential nutrients. Our work demonstrates that the GID/CTLH complex activity broadly suppresses the macrophage's anti-microbial responses and, therefore, represents a tractable target for host-directed therapies (HDTs) in TB control strategies.

Results

FACS-based macrophage survival CRISPR screen to identify intracellular determinants of *Mtb* replication

Infection of macrophages with virulent *Mtb* strains induces necrotic cell death[13,14,21], a virulence mechanism that enables the bacteria to escape the phagosome and spread. To identify genes that contribute to improved macrophage survival after *Mtb* infection, we developed a flow cytometry-activated sorting (FACS)-based CRISPR screen in murine macrophages derived from estradiol responsive Hoxb8 Cas9+ conditionally immortalized myeloid precursors[22] using cytotoxicity as a selection outcome, anticipating that restriction of *Mtb* growth would enhance cell survival. We first optimized *Mtb* cytotoxicity in Hoxb8 bone marrow-derived macrophages (BMDMʰs) at different multiplicity of infections (MOIs). Infection of BMDMʰs with the virulent *Mtb* Erdman strain induced ~50% macrophage cytotoxicity at MOI 1 and >75% cytotoxicity at MOI 3 after 4 days of infection, as measured by the lactate dehydrogenase (LDH) release assay (Fig. 1A). Similar levels of cytotoxicity were evident when we analyzed the infected macrophages by flow cytometry after staining with live dead viability dye (Fig. S1A). As further evidence of bacteria release from dying macrophages, an

MOI-dependent increase in *Mtb* colony forming units (CFUs) was observed in supernatants from the infected macrophage cultures (Fig. 1B). We, therefore, chose a 4-day infection with the *Mtb* Erdman strain at MOI 1 as a selection pressure for our CRISPR screen as it resulted in sufficient proportions of surviving macrophages (Fig. S1A) which can be flow-sorted for downstream library preparation and sequencing. We then transduced Hoxb8 Cas9+ myeloid progenitors with the Brie knockout lentiviral single guide RNA (sgRNA) library[23] that targets ~19,674 mouse protein-coding genes with four sgRNAs/gene. BMDMʰs knockout libraries were differentiated from the Hoxb8 Cas9+ myeloid progenitor library (Fig. S1B) and infected with the *Mtb* Erdman strain at MOI 1 for 4 days. Surviving macrophages based on live dead staining were flow sorted and sequenced to identify candidate genes (Fig. 1C). We carried out the screen in three independent replicates and identified hits by comparing sgRNA read counts in the sample groups to the input unperturbed BMDMʰ library using the MAGeCK-VISPR pipeline (Fig. S2)[24].

We identified 259 genes whose knockout modulated BMDMʰs responses to *Mtb* infection based on a false discovery rate of <0.05 (Fig. 1D, Supplementary Data 1). 104 genes were significantly enriched (conferred relative protection to *Mtb*-induced cytotoxicity), while 155 genes were significantly depleted. The highest-scoring protective hits belonged to the TOR signaling pathway (Fig. 1D, Supplementary Data 1, 2), which has already been implicated in macrophage control of *Mtb*[25]. All the enriched 10 genes in the TOR pathway (*RRAGC, LAMTOR1, RRAGA, TSC1, FLCN, TSC2, LAMTOR4, LAMTOR3, TBC1D7, RPS6KA1*) are part of the mTOR signaling cascade which plays a crucial role in mammalian cell growth and nutrient signaling[26]. These hits are consistent with the literature that mTOR inhibition is known to activate autophagy, a host response that restricts intracellular *Mtb* growth in macrophages[27]. Our hits also included a number of genes and pathways that could negatively impact *Mtb* growth (Fig. 1D, Supplementary Data 2), such as the mitochondrial complex 1 (*NUBPL, TMEM126B, NDUFAF4, NDUFS8, ACAD9, NDUFB9, NDUFC1*), iron-sulfur cluster binding, protein dephosphorylation, regulation of GTPases activity and lysosomal functions. Mitochondrial complex 1 is a target of metformin, a promising HDT against *Mtb*[28] while disruption of iron homeostasis in macrophages by knockout of the iron–sulfur clusters could be restrictive to *Mtb* growth by limiting the bacteria's access to iron[29]. We also identified 5 of the 12 predicted members of the highly conserved mammalian multi-subunit GID/CTLH complex[30,31] (*MAEA, WDR26, UBE2H, YPEL5, GID8*) (Fig. 1D, Supplementary Data 1) as potential determinants of macrophage resistance to *Mtb* driven cell death. Interestingly, 2 of these hits (*WDR26, YPEL5*) were previously identified in a related CRISPR screen in THP1 macrophages using *M. bovis* BCG[20].

Knockout of the GID/CTLH complex in macrophages results in strong intracellular bacteria growth restriction and confers high-level resistance to *Mtb*-induced cell cytotoxicity

The GID/CTLH complex was first identified in yeast as a multi-subunit E3 ligase that targets surplus gluconeogenic enzymes for proteasomal degradation when glucose-starved cells are re-supplied with the substrate[32,33]. In mammals, the complex appears to fulfill other biological functions like cell proliferation and survival, cell migration and adhesion, erythropoiesis, and neurodegenerative diseases[34]. In immunity, some members of the complex (*RANBP9*) have been implicated in antigen processing, efferocytosis, and anti-inflammatory activities[35,36]. We generated de novo knockouts in Hoxb8 Cas9+ myeloid progenitors for the five GID/CTLH hits identified in our screen (*MAEA, WDR26, UBE2H, YPEL5, GID8*), which represent ~50% of the predicted functional members of the complex in humans and mice[30]. We targeted each gene with 2 sgRNAs and were able to achieve >85% knockout efficiencies (Supplementary Data 3) as analyzed by the Inference of CRISPR Edits (ICE) tool[37]. Similar levels of protein
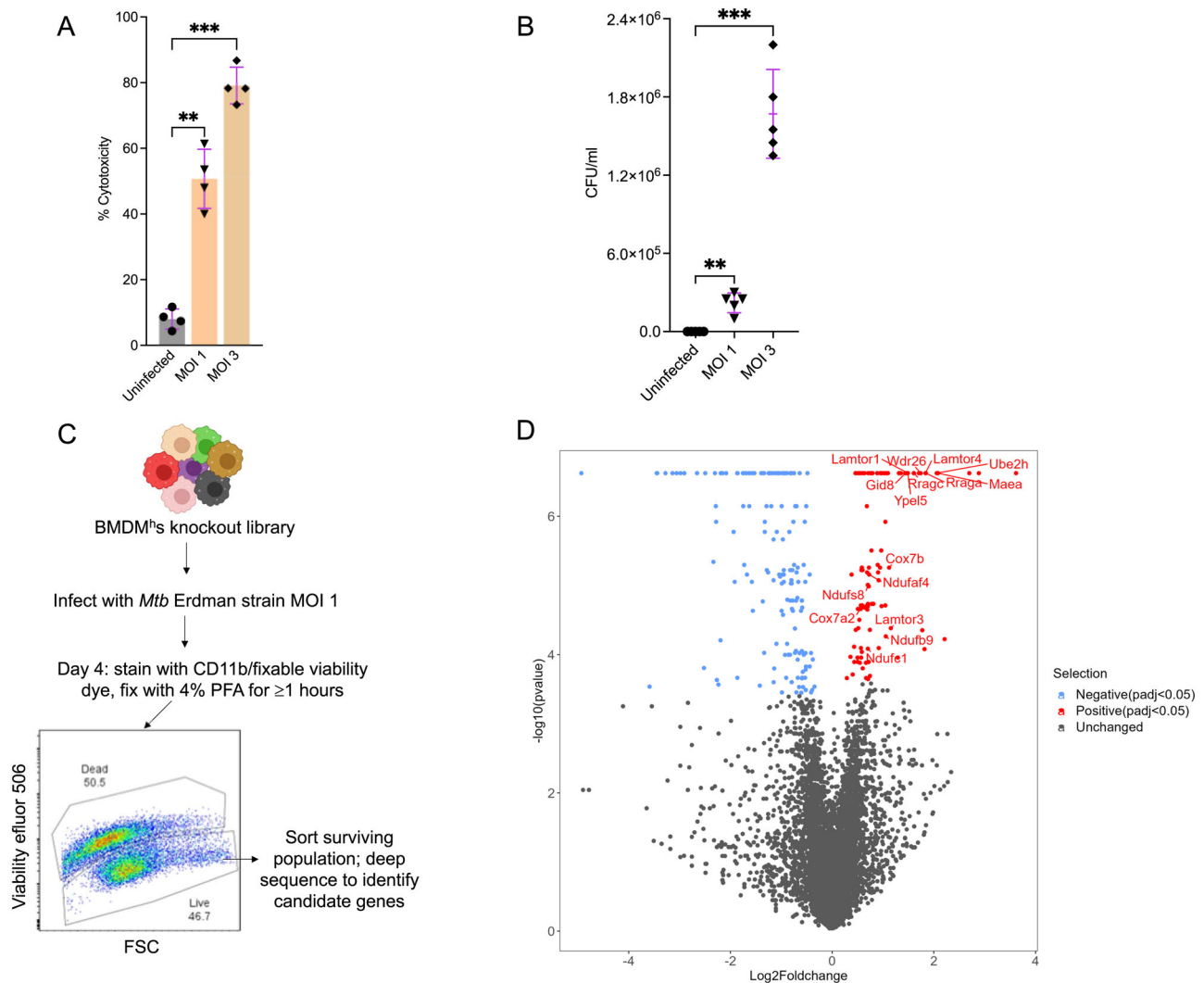
Fig. 1 | Genome-wide CRISPR screen to identify host determinants of tuberculosis restriction in macrophages. A *Mycobacterium tuberculosis* (*Mtb*) induced cytotoxicity in Hoxb8 bone marrow-derived macrophages (BMDM[h]s) at the indicated multiplicity of infections (MOI) 4 days post infection. Cytotoxicity was quantified by measuring the activity of released lactate dehydrogenase (LDH) in cell supernatants as compared to 100% LDH activity in detergent-lysed cells; $n = 4$ biological replicates. **$P < 0.01$; ***$P < 0.001$, one-way ANOVA alongside Dunnett's multiple comparison test. Data are presented as mean values ± SD. **B** A further quantification of *Mtb* induced cytotoxicity in macrophages at indicated MOIs by plating colony forming units (CFUs) in cell supernatants from experimental conditions as in (**A**); $n = 5$ biological replicates. **$P < 0.01$; ***$P < 0.001$, one-way ANOVA alongside Dunnett's multiple comparison test. Data are presented as mean values ± SD. **C** Schematic workflow for performing CRISPR screen to identify host determinants of *Mtb* restriction in macrophages. Part of this graphic was created in BioRender. Lee, B. (2024) BioRender.com/t32i914. **D** Volcano plot showing hits from the screen. For each gene (represented by dots), enrichment or depletion is shown in the x axis as log2 fold change while the y axis shows the corresponding −log10 p value. Significantly enriched and depleted hits are shown in red and blue colors, respectively, while unchanged hits are in gray. For significant hits, an adjusted p value of <0.05 was used as a cutoff. Screens were carried out in three independent replicates. Source data are provided as a Source Data file.

knockout were also confirmed by western blot analysis for all five genes in BMDM[h]s differentiated from the Hoxb8 Cas9^{+} mutants (Fig. S3). We then infected the GID/CTLH knockout BMDM[h]s (*GID8*^{−/−}, *YPEL5*^{−/−}, *WDR26*^{−/−}, *UBE2H*^{−/−}, *MAEA*^{−/−}) differentiated from the Hoxb8 Cas9^{+} mutants with the *Mtb* Erdman strain at MOI 0.4 for 4 days to determine the intracellular growth replication rates of *Mtb* in these macrophages. An MOI of 0.4 was chosen to minimize macrophage cell death on the day of plating CFUs in accordance with prior optimizations (Fig. 1B, S1A). A strong *Mtb* growth restriction was observed in all the five GID/CTLH mutants as compared to macrophages transduced with a non-targeting scramble sgRNA control (Fig. 2A). The growth restriction phenotypes were not due to differences in bacteria uptake or phagocytosis defects as there were no significant differences when we plated CFUs 3 hours post infection (Fig. 2A). Similar intracellular growth restriction phenotypes were observed when we infected

selected mutants (*MAEA*^{−/−}, *GID8*^{−/−}, *WDR26*^{−/−}) with the *Mtb* Erdman-Lux reporter strain and monitored bacterial growth by luciferase expression (Fig. 2B).

We also analyzed the growth restriction phenotypes of the GID/CTLH knockout BMDM[h]s using another intracellular bacterium, *Salmonella enterica* serovar Typhimurium (*S.* Typhimurium), in the gentamicin protection assay[38]. *MAEA*^{−/−} and *GID8*^{−/−} knockout BMDM[h]s were infected with the wild-type *S.* Typhimurium ATCC 14028s strain at MOI 10, and CFUs were plated 4 and 18 hours post infection. Again, we observed a strong intracellular growth restriction of *S.* Typhimurium in these mutant macrophages, compared to scramble sgRNAs (Fig. S4A). The growth restriction phenotypes were also not due to bacterial uptake differences as similar bacteria numbers were evident in scramble and mutant macrophages infected with the isogenic BFP-expressing *S.* Typhimurium strain, *phoN*::BFP[39] for 1-hour, as analyzed
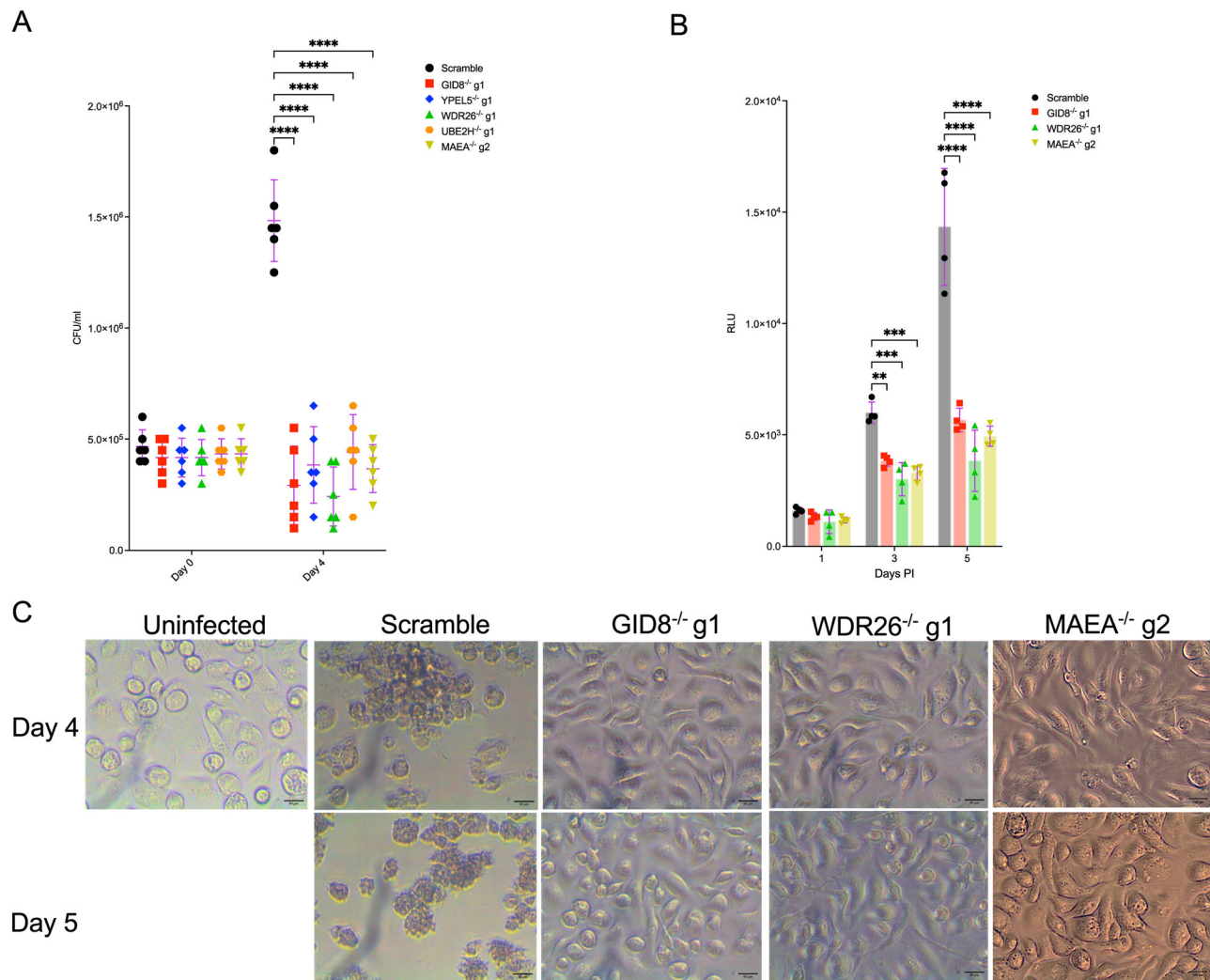
Fig. 2 | Macrophages with knockout of the GID/CTLH complex are strongly restrictive to *Mtb* intracellular growth and are resistant to *Mtb*-induced cell death. A Wild-type (scramble) or indicated GID/CTLH knockout BMDMʰs were infected with *Mtb* Erdman strain at MOI 0.4. CFUs were plated on day 0 (3 hours post infection) and on Day 4 to determine intracellular *Mtb* replication rates; *n* = 6 biological replicates. ****P < 0.001, two-way ANOVA alongside Dunnett's multiple comparison test. Data are presented as mean values ± SD. **B** Quantification of *Mtb* replication in scramble or *GID8⁻/⁻*, *MAEA⁻/⁻*, and *WDR26⁻/⁻* BMDMʰs using the *Mtb* Erdman-Lux strain. BMDMʰs were infected at MOI 0.5, following which luciferase measurements were taken on the indicated days; *n* = 4 biological replicates. **P < 0.01; ***P < 0.001; ****P < 0.0001, two-way ANOVA alongside Dunnett's multiple comparison test. Data are presented as mean values ± SD. **C** Microscopy micrographs of scramble or *GID8⁻/⁻*, *MAEA⁻/⁻*, and *WDR26⁻/⁻* BMDMʰs infected with *Mtb* Erdman strain at MOI 1 taken on day 4 and 5 post-infection. Source data are provided as a Source Data file.

by confocal microscopy (Fig. S4B, C). To confirm that intracellular bacterial growth restriction phenotypes of GID/CTLH knockout in macrophages were conserved in human cells, we generated *GID8* and *MAEA* knockouts in primary human monocyte-derived macrophages (hMDMs) by directly electroporating CRISPR ribonucleoproteins (CRISPR RNPs) in monocytes[40]. We targeted each gene with at least 2 sgRNAs and were able to achieve 50–70% knockout efficiencies with some sgRNAs, specifically sgRNA 2 for *hGID8⁻/⁻* and sgRNA 1 for *hMAEA⁻/⁻* (Fig. S5A, Supplementary Data 3). More importantly, we observed *Mtb* growth restriction levels that were dependent on the degree of protein knockout in these hMDM mutants by both CFUs and luciferase readouts (Fig. S5B, C). These data illustrated the functional conservation of the GID/CTLH complex in mediating intracellular growth restriction of bacteria in both mice and humans.

To assess GID/CTLH knockout BMDMʰs ability to resist *Mtb*-induced cell death, which was a key feature of our CRISPR screening strategy, we analyzed the mutant macrophages cell death kinetics upon infection with the *Mtb* Erdman strain at MOI 1 by microscopy 4- and 5-days post infection. *Mtb* infection induced macrophage death

that resulted in about half of the cells appearing necrotic by day 4 in scrambled sgRNA macrophages (Fig. 2C), which is consistent with LDH and flow cytometry-based quantifications (Figs. 1A and S1A). Almost all the cells in the scramble control appeared necrotic by day 5 (Fig. 2C). However, GID/CTLH knockout macrophages were highly resistant to cell death with 100% survival rates on days 4 and 5. Together, these data suggested that the knockout of the GID/CTLH complex does not just restrict the intracellular growth of *Mtb* in macrophages but also inhibits necrotic cell death programs triggered by the bacteria.

We investigated whether knockout of other members of the GID/CTLH complex that were not identified in the primary screen also impacted *Mtb* growth in BMDMʰs by generating *RANBP9⁻/⁻* and MKLN1⁻/⁻ knockouts (Fig. S6A, Supplementary Data 3) and assessing bacterial growth upon infection with the *Mtb* Erdman-Lux reporter strain at MOI 0.5. We observed significant *Mtb* growth restriction in *RANBP9⁻/⁻* and *MKLN1⁻/⁻* knockout BMDMʰs 4 days post-infection when compared to scramble sgRNA (Fig. S6B). *RANBP9⁻/⁻* and *MKLN1⁻/⁻* BMDMʰs also displayed increased resistance to *Mtb* induced cell death when infected with the *Mtb* wild-type Erdman strain at MOI 1 for 4 days

(Fig. S6C). The levels of *Mtb* growth restriction and resistance to cell death in *RANBP9*^{-/-} and *MKLN1*^{-/-} BMDM[h]s were lower than the GID/CTLH members identified in the screen (Fig. 2). The design of the screen clearly favored those members of the complex which, upon knockout, resulted in strongest anti-bacterial phenotypes.

Mtb-infected GID/CTLH knockout macrophages are metabolically resilient and more glycolytically active

In yeast, the GID/CTLH complex is directly involved in glucose metabolism by regulating gluconeogenesis[32]. Even though some studies have shown that the complex is dispensable in the regulation of carbohydrate metabolism in human cells[30], others have identified glycolytic enzymes L-lactate dehydrogenase A chain (LDHA) and pyruvate kinase M1/2 (PKM) as direct targets of GID/CTLH ubiquitination[41]. In fact, depletion of the GID/CTLH complex member *RMND5A* reduces polyubiquitination of LDHA and PKM and renders the cells more glycolytic[41]. Moreover, the GID/CTLH complex (member *RMND5A*) appears to regulate cell energy homeostasis by negatively modulating the activity of the AMP-activated protein kinase (AMPK)[42]. We therefore profiled the metabolic state of a selected GID/CTLH knockout BMDM[h]s (*GID8*^{-/-}, *MAEA*^{-/-} and *WDR26*^{-/-}) in uninfected or *Mtb* infected conditions. We chose to characterize these 3 mutants further because, amongst the GID/CTLH complex members, *GID8* or *TWA1* is a scaffold that holds the complex together, *MAEA* forms part of the catalytic core[30], and *WDR26* was identified in a previous related screen[20] and is also predicted to be central to the core structure of the complex[30]. We first checked the relative mRNA expression of the glycolytic enzyme hexokinase 2 (*Hk2*) and the gluconeogenic enzyme fructose-1,6-bisphosphatase 1 (*FBP1*) in these GID/CTLH knockout BMDM[h]s. We observed a significant increase in mRNA expression of *HK2* in uninfected GID/CTLH knockout BMDM[h]s as compared to scramble (Fig. S7A). *Mtb* infection maintained a higher expression of *HK2* in GID/CTLH knockout BMDM[h]s 4 hours post infection as compared to scramble, but these responses resolved after 24 hours of infection (Fig. S7A). This is consistent with a biphasic metabolic profile of macrophage responses to *Mtb* infection, which is characterized by an early upregulation of glycolytic genes in the first 4−8 hours of infection that diminishes 24−48 hours later[43]. We did not, however, observe any differences in *FBP1* expression in uninfected or *Mtb* infected GID/CTLH knockout BMDM[h]s (Fig. S7A). These results suggest that GID/CTLH knockout in BMDM[h]s does not impact gluconeogenesis (at least at the transcript level) but programs the cells to a more glycolytic state, which is consistent with previous observations[41].

To further confirm these phenotypes, we analyzed the metabolic status of GID/CTLH knockout BMDM[h]s by Seahorse extracellular flux analyses using the Agilent Mito and Glycolysis Stress Test kits. Compared to scramble sgRNA, uninfected GID/CTLH knockout BMDM[h]s displayed increased basal oxygen consumption rates (OCRs) and reduced spare respiratory capacity (SRC) (Fig. S7B, C) which suggested impacted mitochondrial activities and oxidative phosphorylation as a consequence of GID/CTLH knockout. In agreement with our qPCR data (Fig. S7A), we also observed increased glycolytic flux in uninfected GID/CTLH knockout BMDM[h]s as evidenced by high basal extracellular acidification rates (ECAR) and spare glycolytic capacity (SGC) (Fig. S7D). Under basal conditions, *Mtb* infection of wild type macrophages increases glycolytic rates that are required to control bacterial replication[44] while at the same time decelerates mitochondrial respiration[45]. Indeed, when we infected scramble macrophages with *Mtb* for 24 hours, SRC rates collapsed to almost baseline levels (Fig. 3A, B) compared to uninfected cells (Fig. S7B, C). However, *Mtb* infected GID/CTLH knockout macrophages were more resilient as they maintained significantly higher basal OCRs and SRCs as compared to scramble sgRNA (Figs. 3A, B, S7C). Glycolytic rates in *Mtb* infected GID/CTLH knockout BMDM[h]s were also significantly higher as compared to scramble sgRNA (Fig. 3C, D) albeit at an even higher rate than the

uninfected (Fig. S7D). Together, our qPCR and extracellular flux analysis data demonstrated that knockout of the GID/CTLH complex in macrophages impairs mitochondrial respiration and proportionally increases flux through glycolysis. However, GID/CTLH knockout BMDM[h]s are able to withstand an *Mtb*-induced bioenergetic shutdown[45] despite displaying reduced spare mitochondrial capacity in uninfected conditions.

Our metabolic analyses also pointed to a state of energy stress in GID/CTLH knockout BMDM[h]s, which could be regulated, in part, by AMPK, a master regulator of cell energy homeostasis[46]. Given that AMPK can be modulated (negatively) by the GID/CTLH complex[42], we also checked AMPK activity in uninfected and *Mtb*-infected GID/CTLH knockout macrophages by monitoring the levels of total and activated (phosphorylated) AMPK in western blot analyses. Both uninfected and *Mtb* infected GID/CTLH knockout macrophages displayed reduced expression of total AMPK (Figs. 3E and S8A−C), which could possibly explain reduced SRC rates of these mutants at least in uninfected states (Fig. S7B). We, however, observed increased AMPK phosphorylation in both uninfected and *Mtb*-infected GID/CTLH knockout macrophages (Figs. 3E, F and S8A, B), and the P-AMPK/AMPK ratios were significantly higher in the mutants (Fig. 3G).

Dual RNA-sequencing identifies GABAergic signaling and autophagy as major host determinants of *Mtb* restriction in GID/CTLH knockout BMDM[h]s

To further identify effectors that mediate *Mtb* growth restriction in GID/CTLH knockout BMDM[h]s, we performed dual RNA-sequencing (dual RNA-seq) of *Mtb*-infected knockout macrophages to capture both host and bacterial transcriptomes[47]. Scramble sgRNAs or GID/CTLH knockout BMDM[h]s (*GID8*^{-/-}, *MAEA*^{-/-}, *WDR26*^{-/-}) were infected with the *Mtb* smyc'::mCherry strain for 4 days. On day 4, we flow-sorted infected macrophages based on mCherry positivity and extracted RNA for dual RNA-seq[47]. Principal component analysis (PCA) of the macrophage transcriptomes revealed unique clustering of *GID8*^{-/-}, *MAEA*^{-/-} and *WDR26*^{-/-} BMDM[h]s which, despite being slightly distant from each other, clustered close together in the first principal component as compared to scramble sgRNA (Fig. 4A). Using an adjusted *p* value of <0.05 and an absolute log2 fold change of > 0.5, we identified 1911 upregulated and 918 downregulated genes in *GID8*^{-/-} macrophages, 2106 upregulated and 940 downregulated genes in *MAEA*^{-/-} macrophages and 2890 upregulated and 1845 downregulated genes in *WDR26*^{-/-} macrophages (Supplementary Data 4). Due to the similar separation of *GID8*^{-/-}, *MAEA*^{-/-} and *WDR26*^{-/-} in our PCA analysis (Fig. 4A), we generated a Venn diagram to identify differentially expressed (DE) genes in common between the three mutant macrophage populations. Indeed, the majority of DE genes (1267 upregulated, 421 downregulated) were present in the *GID8*^{-/-}, *MAEA*^{-/-} and *WDR26*^{-/-} *Mtb* infected BMDM[h]s (Fig. 4B, C, Supplementary Data 4). Among the highly upregulated genes in the commonly DE gene set were those involved in macrophage effector functions that are known to control *Mtb* replication, such as the NADPH oxidase (*NOX3*) and autophagy (*ATG9B, TRIM2, TRIM7, and TRIM16*) (Supplementary Data 4). Ferroportin 1 (*SLC40A1*), the only known membrane protein to transport iron out of the cells[48], was also among the most significantly upregulated genes in *GID8*^{-/-}, *MAEA*^{-/-} and *WDR26*^{-/-} *Mtb* infected BMDM[h]s (Supplementary Data 4). This suggested that GID/CTLH knockout in BMDM[h]s could restrict *Mtb* growth by nutrient (iron) limitation, enhancing autophagy and increasing the production of reactive oxygen species (ROS). Given that the role of the GID/CTLH complex in macrophage anti-microbial functions is mostly unknown, we used our RNA-seq results to check the expression status (at transcript level) of the 12 GID/CTLH members, at least in wild-type (scramble) *Mtb* infected macrophages. We detected transcripts for all 12 members of the GID/CTLH complex, which suggests active expression of the entire complex in myeloid cells (Fig. S9A).
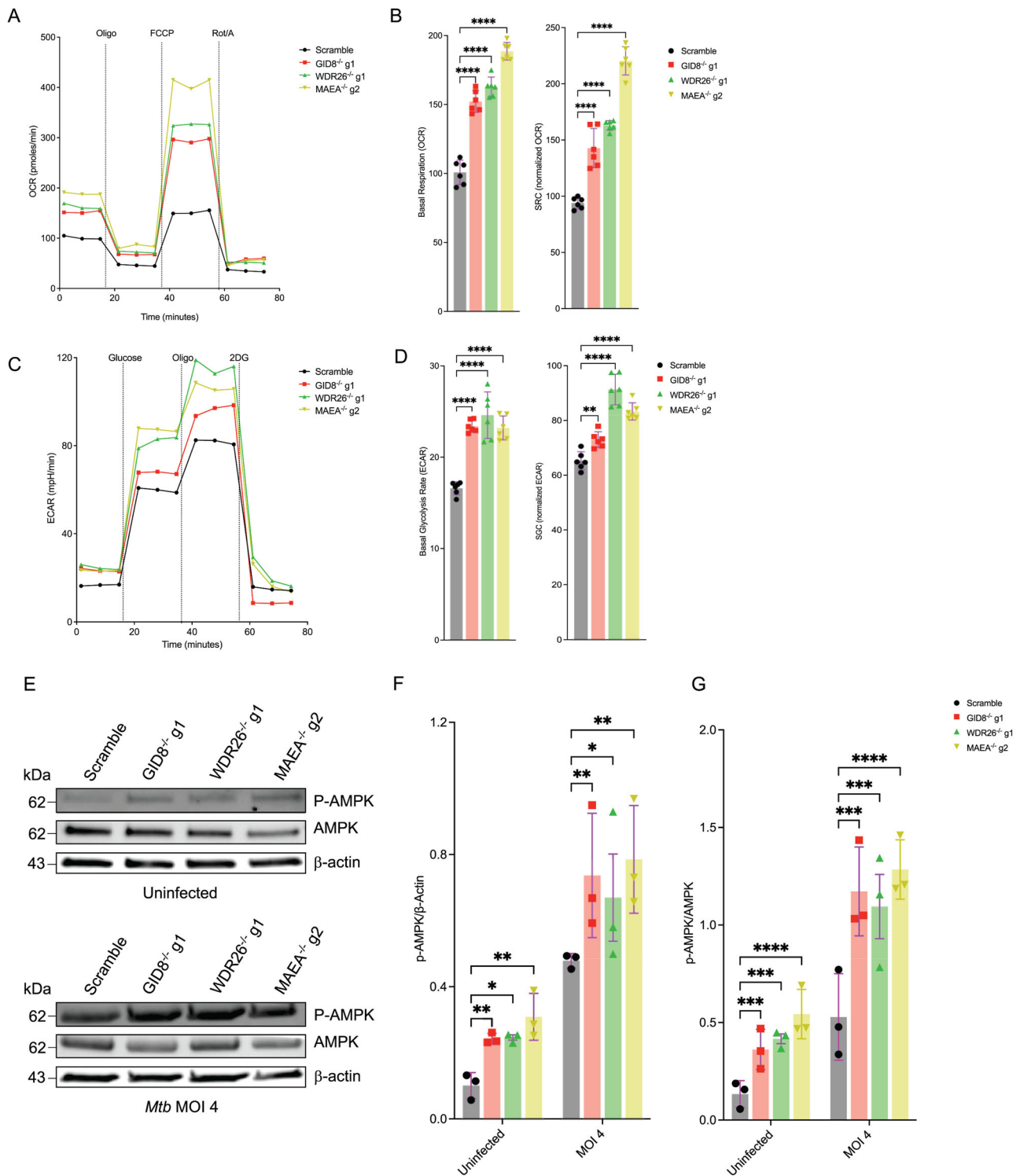
Fig. 3 | *Mtb* infected GID/CTLH knockout macrophages have altered metabolism and are strongly glycolytic. A Flux analyses of scramble or *GID8$^{-/-}$*, *MAEA$^{-/-}$* and *WDR26$^{-/-}$* BMDM^{h}s infected with *Mtb* Erdman strain at MOI 1 24 hours post infection. Oxygen consumption rates (OCR) were measured using the Cell Mito Stress Test Kit (Agilent). Oligo, oligomycin; FCCP, fluoro-carbonyl cyanide phenylhydrazone; Rot/A, rotenone and antimycin A. **B** Comparison of basal respiration and spare respiratory capacity (SRC) from (**A**). SRC was calculated by subtracting the normalized maximal OCR from basal OCR; $n = 3$ biological replicates (two technical replicates per repeat). ****$P < 0.0001$, one-way ANOVA alongside Dunnett's multiple comparison test. Data are presented as mean values ± SD. **C** Extracellular acidification rates (ECARs) of scramble or *GID8$^{-/-}$*, *MAEA$^{-/-}$* and *WDR26$^{-/-}$* BMDM^{h}s infected with *Mtb* as in (**A**). ECARs were measured using the Agilent Seahorse Glycolysis Stress Test kit. 2DG, 2-Deoxy-D-glucose. **D** Comparison of basal glycolysis and spare glycolytic capacity (SGC) in the indicated BMDM^{h} knockouts. SGC was calculated as SRC above. $n = 3$ biological replicates (two technical replicates per repeat). **$P < 0.01$; ****$P < 0.0001$, one-way ANOVA alongside Dunnett's multiple comparison test. Data are presented as mean values ± SD. **E** Western blot analysis of AMPK phosphorylation in scramble or *GID8$^{-/-}$*, *MAEA$^{-/-}$*, and *WDR26$^{-/-}$* BMDM^{h}s uninfected or infected with *Mtb* at MOI 4. **F** Quantification of relative expression of p-AMPK in (**E**) and in Fig. S8A, B normalized to β-actin; $n = 3$ biological replicates. *$P < 0.05$; **$P < 0.01$, two-way ANOVA alongside Dunnett's multiple comparison test. Data are presented as mean values ± SD. **G** p-AMPK/ AMPK ratios of relative expressions in (**E**) and in Fig. S8A, B as normalized to β-actin; $n = 3$ biological replicates. ***$P < 0.001$; ****$P < 0.0001$, two-way ANOVA alongside Dunnett's multiple comparison test. Data are presented as mean values ± SD. Source data are provided as a Source Data file.
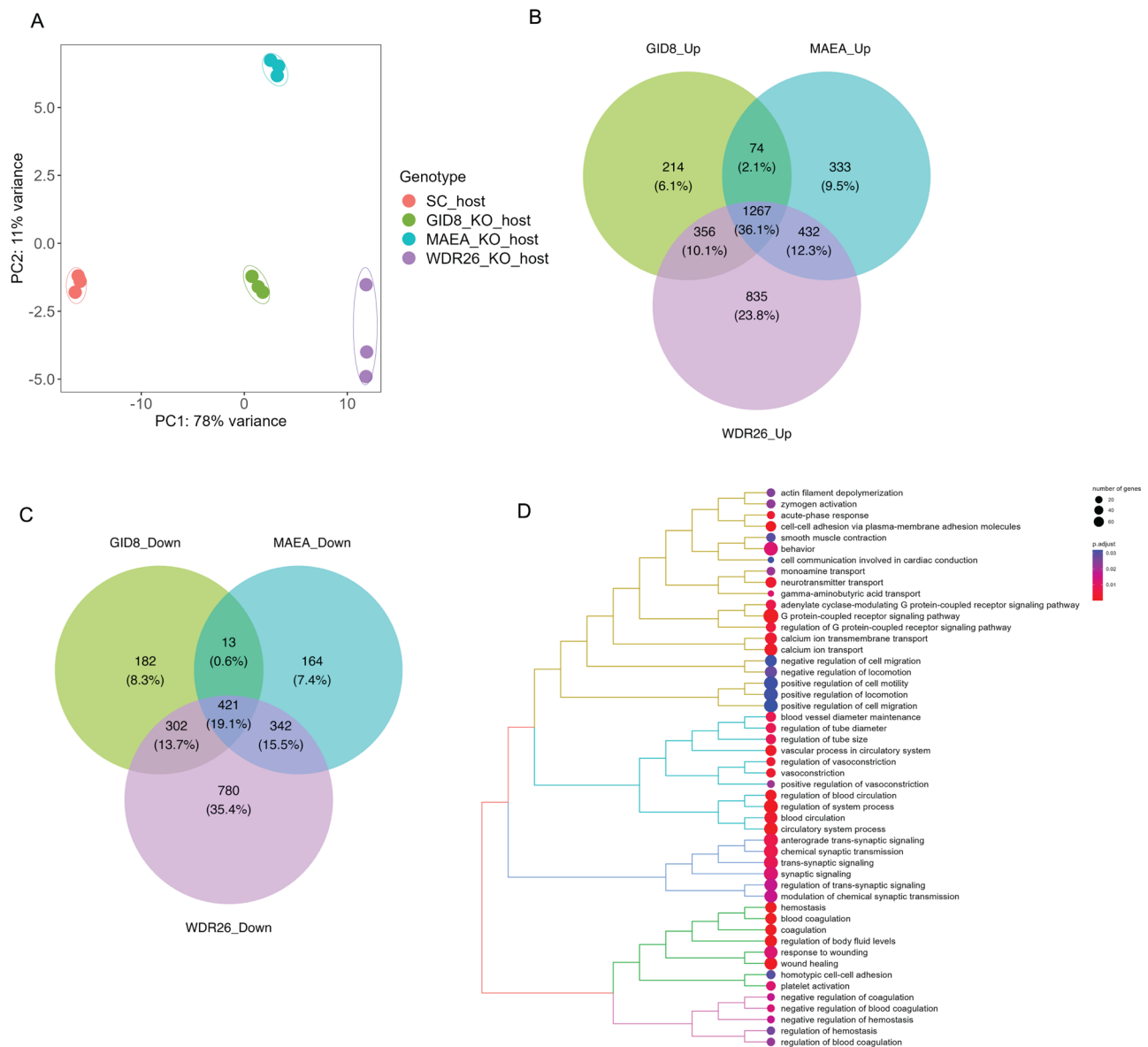
Fig. 4 | Host transcriptional responses to identify determinants of *Mtb* restriction in GID/CTLH knockout macrophages. A Principal component analysis (PCA) of scramble or *GID8⁻/⁻*, *MAEA⁻/⁻* and *WDR26⁻/⁻* knockout host (BMDMʰs) transcriptomes infected with the *Mtb* smyc'::mCherry strain at MOI 0.5 4 days post infection. **B**, **C** Venn diagrams of upregulated and downregulated gene sets (Supplementary Data 4) in *GID8⁻/⁻*, *MAEA⁻/⁻* and *WDR26⁻/⁻* BMDMʰs as compared to scramble showing overlapping genes. Differentially expressed genes cutoff; abs (log₂ fold change) >0.5, adjusted *p* value < 0.05. **D** Tree plot of top 50 enriched gene ontology terms (biological process) amongst the 1267 commonly upregulated genes in *GID8⁻/⁻*, *MAEA⁻/⁻*, and *WDR26⁻/⁻* BMDMʰs.

To gain more insights into biological pathways that could mediate *Mtb* growth restriction in GID/CTLH knockout macrophages, we performed pathway enrichment analysis[49] of the *GID8⁻/⁻*, *MAEA⁻/⁻* and *WDR26⁻/⁻* commonly DE genes (Supplementary Data 4). In the upregulated gene set, we identified 60 biological processes (BP), 30 cellular components (CC), and 27 molecular functions (MF), which were enriched based on an adjusted *p* value of <0.05 (Fig. 4D, Supplementary Data 5). Amongst the commonly downregulated DE genes, 332 BP, 16 CC, and 44 MF were enriched (Fig. S9B, Supplementary Data 5). Of the top enriched BPs in the commonly upregulated genes (Fig. 4D), the most enriched pathways included those involved in Ca²⁺ and G protein receptor signaling, effector processes that are known to play important roles in macrophage responses against *Mtb*[50,51]. Of note, γ-Aminobutyric acid (GABA) and neurotransmitter transport were, similarly, amongst the most enriched pathways in the GID/CTLH knockout upregulated genes (Fig. 4D, Supplementary Data 5). Within the GID/CTLH complex,

only one member (Muskelin, *MKLN1*) has been shown to be involved in GABA receptor trafficking and internalization[52]. We, however, identified six genes in the GABAergic signaling pathway (*GABBR1*, *GABRB2*, *GABARAPL1*, *SLC32A1*, *SLC6A13*, *SLC6A12*) which were upregulated in all the three *Mtb* infected GID/CTLH knockout mutants; *GID8⁻/⁻*, *MAEA⁻/⁻* and *WDR26⁻/⁻* (Supplementary Data 4 and 5). In fact, *GABBR1* and *GABRB2* were amongst the most significantly upregulated genes in the GID/CTLH knockout macrophages with up to 350-fold upregulation as compared to scramble sgRNA (Supplementary Data 4). GABAergic signaling has recently been linked to intracellular macrophage control of *Mtb* and *S.* Typhimurium. Treatment of macrophages with GABA or GABAergic drugs enhances the anti-microbial properties of macrophages against intracellular bacterial infections by promoting phagosome maturation and autophagy[53]. Moreover, the apparent GABAergic protective responses in BMDM macrophages were driven, in significant part, by an increase in Ca²⁺ signaling[53]. Taken together, our pathway

enrichment data suggested that GID/CTLH knockout in BMDM^{h}s increases GABA and Ca^{2+} signaling, which may, similarly, promote macrophage control of *Mtb* by promoting autophagy[53]. A further consequence of GABA treatment in *Mtb* infected BMDMs and in infected mice lungs in vivo was the inhibition of pro-inflammatory markers such as Tnf and IL-6[53]. Similarly, pro-inflammatory pathways were the most significantly enriched pathways in our GID/CTLH commonly downregulated genes (Fig. S9B, Supplementary Data 5). These included pathways involved in IL-1β production, antigen presentation, toll receptor signaling, and cellular responses to Tnf. Our further analysis of the RNA-seq data did indeed show significant downregulation of IL-1β and Tnf transcripts in all the GID/CTLH knockout macrophages infected with *Mtb* on day 4 (Fig. S9C). Consistent with the known role of the GID/CTLH complex in cell proliferation[34], pathways related to DNA replication were also among the most enriched in the downregulated gene set (Fig. S9B). We also observed a significant downregulation of pathways related to cell death programs and apoptosis signaling (Supplementary Data 5) in GID/CTLH knockout BMDM^{h}s, which would possibly explain the increased resistance of these macrophages to *Mtb*-induced cytotoxicity (Fig. 2C).

Nutritional stress is the main transcriptome signature of intracellular *Mtb* in GID/CTLH knockout BMDM^{h}s

To assess the impact of host stressors on *Mtb*, we analyzed parallel transcriptomes of intracellular *Mtb* (Fig. 4A). Using an adjusted *p* value of <0.05 and an absolute log2 fold change of >0.3, we identified 168 *Mtb* genes (87 upregulated, 81 downregulated) in $GID8^{-/-}$ BMDM^{h}s, 40 *Mtb* genes (13 upregulated, 27 downregulated) in $MAEA^{-/-}$ BMDM^{h}s and 46 *Mtb* genes (22 genes upregulated, 26 downregulated) in $WDR26^{-/-}$ BMDM^{h}s which were DE (Fig. 5A, Supplementary Data 6). Interestingly, clusters of upregulated *Mtb* genes in these GID/CTLH knockout BMDM^{h}s were readily categorized into essential *Mtb* biological processes such as iron scavenging, cholesterol breakdown, fatty acid oxidation, amino acid metabolism and stress responses (Fig. 5B). *Mtb* utilizes Fe^{3+} iron specific siderophores, mycobactins and carboxymycobactins, to scavenge and acquire iron from the host for its
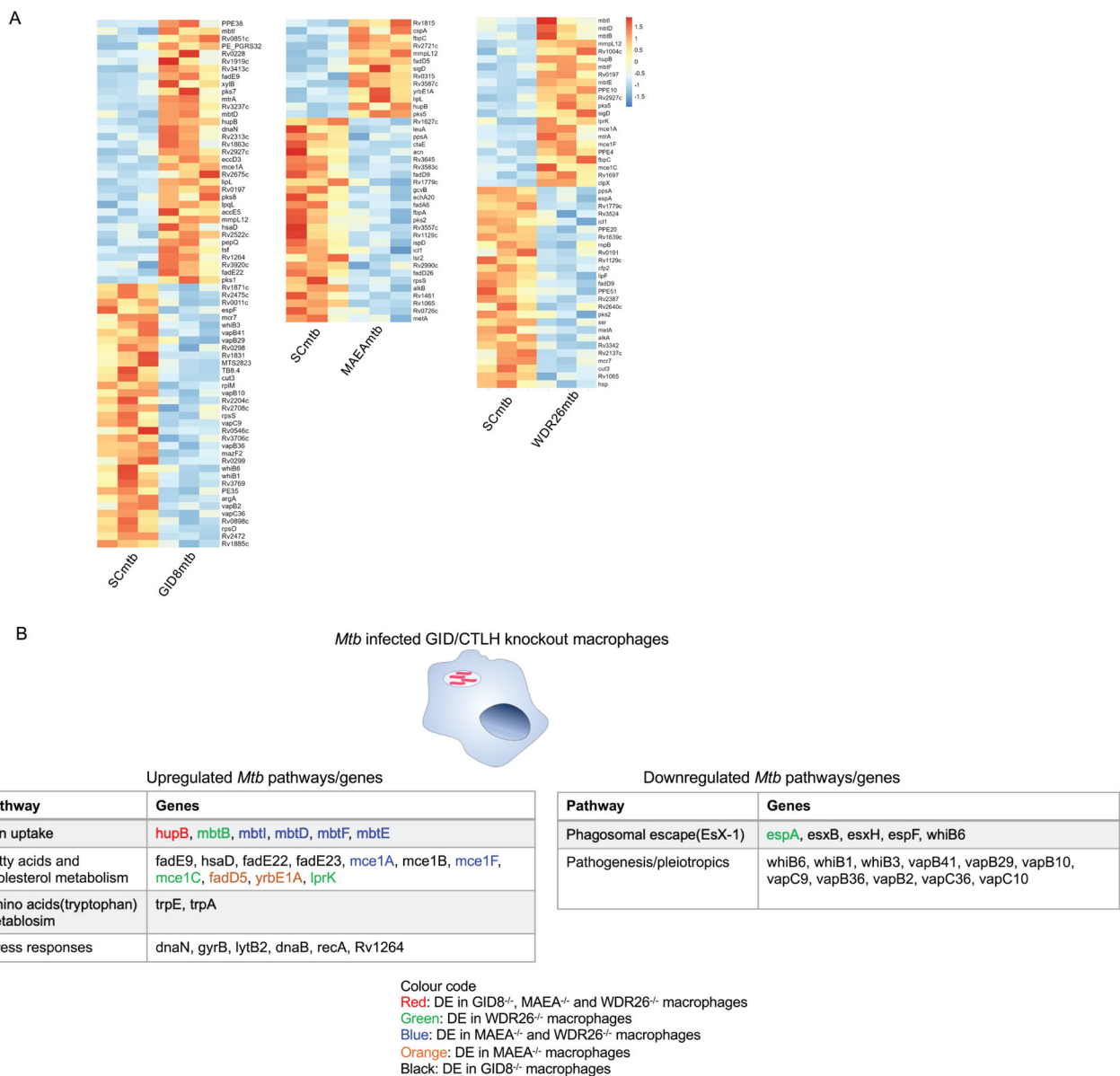

Fig. 5 | *Mtb* transcriptional responses in GID/CTLH knockout macrophages. A Heatmaps of the top differentially expressed genes in *Mtb* isolated from $GID8^{-/-}$ (70 genes), $MAEA^{-/-}$ (40 genes), and $WDR26^{-/-}$ (50 genes) BMDM^{h}s. **B** Schematic of some of the differentially expressed genes in *Mtb* isolated from $GID8^{-/-}$, $MAEA^{-/-}$, and $WDR26^{-/-}$ BMDM^{h}s categorized into pathways.

nutritional requirements. *Mtb* mycobactins are organized into a cluster of *Mbt* (*MbtA-MbtJ*) and *Mbt-2* (*MbtK-MbtN*) genes[54]. We identified five genes in the *Mbt* cluster (*MbtB, MbtI, MbtD, MbtE, MbtF*) which were upregulated in *Mtb* transcriptomes isolated from GID/CTLH knockout BMDM[h]s (Fig. 5B, Supplementary Data 6). A positive regulator of *Mbt* operonic gene expression, *HupB*[55], was also upregulated in all the three *Mtb* transcriptomes isolated from GID/CTLH knockout macrophages (Fig. 5B, Supplementary Data 6). These data suggested that GID/CTLH knockout macrophages, in part, limit intracellular *Mtb* growth by reducing the bacteria's access to iron. This is consistent with our host transcriptome data which showed a significant upregulation of the iron efflux transporter (*SLC40A1*) in GID/CTLH knockout macrophages (Supplementary Data 4). The data is also consistent with our previous findings, which have shown that iron limitation is one of the prominent stresses experienced by *Mtb* in vivo in lung interstitial macrophages, which are less permissive to *Mtb* growth[47] and that similar *Mtb*-restrictive phenotypes can be reproduced in human macrophages using iron chelating chemical inhibitors[29]. *Mtb* nutrient limitation in GID/CTLH knockout macrophages was not limited to iron as we also observed an upregulation of genes involved in beta-oxidation of fatty acids (*FadE9, FadD5, FadE22, FadE23*)[56], cholesterol breakdown (*HsaD*)[57] and several members of the *Mce1* operon (*Mce1A, Mce1B, Mce1F, Mce1C, yrbE1A, lprK*), which is required for *Mtb* fatty acid import[58,59]. Our previous work has demonstrated that limiting *Mtb*'s access to iron can upregulate cholesterol metabolism genes to re-balance impaired metabolic fluxes that arise due to diminished activity of iron-dependent metabolic pathways[29]. Even though upregulation of *Mtb* lipid metabolism genes in GID/CTLH knockout macrophages could, indeed, be a compensatory mechanism to iron limitation[29], *Mtb* nutrient restriction in these macrophages appears to be more pervasive as the bacteria also upregulates genes involved in tryptophan biosynthesis pathways (*TrpE, TrpA*) (Fig. 5B, Supplementary Data 6). *Mtb* scavenges tryptophan from its host macrophage, however, upon immune activation, the macrophage turns on its tryptophan degradation pathway, and the bacteria respond by upregulation of its tryptophan biosynthetic genes[60,61]. GID/CTLH knockout macrophages also appear to induce other non-nutritional stresses to intracellular *Mtb* as evidenced by the upregulation of genes required to enhance survival at low pH in the phagosome (*Rv1264*)[62]. *Mtb* DNA damage and repair genes (*DnaN, DnaB, gyrB, recA*) (Fig. 5B) were also upregulated, which is indicative of increased oxidative stress as we have previously observed in *Mtb* isolated from growth-restrictive interstitial macrophages in vivo[47].

Interestingly, *Mtb* in GID/CTLH knockout macrophages downregulated major virulence genes, including those belonging to the *ESX-1* type VII secretion system (Fig. 5B). We identified 4 genes in the *ESX-1* operon (*espA, esxB, esxH, espF*) which were significantly downregulated in *Mtb* isolated from GID/CTLH knockout macrophages. A further three genes (*WhiB1, WhiB3, WhiB6*) belonging to the *WhiB*-like family of transcription factors that play key roles in *Mycobacteria* virulence and antibiotic resistance[63] were also significantly downregulated (Fig. 5B, Supplementary Data 6). Of note, *WhiB6* is one of the main regulators of *ESX-1* gene expression in *Mtb*[64,65]. Central to the activity of all *WhiB* transcription factors are highly conserved cysteine-bound iron-sulfur clusters that can act as reductive sinks to host nitric oxide or ROS produced during macrophage activation[63]. It has been demonstrated that disruption of iron-sulfur clusters in *WhiB* transcription factors either by iron limitation or excessive nitrosative stress can trigger a significant reprogramming of gene expression in *Mtb*[66]. Downregulation of *Mtb WhiB* genes in GID/CTLH knockout macrophages could also, therefore, be a result of iron-limiting conditions in these mutant phagocytes, which in the case of *WhiB6* could trigger a feed-forward effect to downregulate downstream *ESX-1* genes. As a consequence of *ESX-1* downregulation, *Mtb* resident in GID/CTLH knockout macrophages may be attenuated and possibly

trapped in phagosomes, given the role of this secretion system in *Mtb* virulence and phagosomal escape[15]. Several toxin-antitoxin (TA) genes were also downregulated in *Mtb* isolated from GID/CTLH knockout macrophages (Fig. 5B, Supplementary Data 6). Despite a reductive evolution in the *Mtb* genome, TA systems have been maintained to support *Mtb* replication, virulence and stress adaptation[67]. Reduced expression of *Mtb* TA genes in GID/CTLH knockout macrophages could thus be a further indication of shutdown in most bacterial virulence processes in parallel with the observed growth restriction phenotypes (Figs. 2A, B).

GID/CTLH knockout macrophages display increased GABAergic and Ca²⁺ signaling

We followed up on our dual RNA-seq data (Fig. 4) to experimentally validate some of the host effectors that mediate *Mtb* growth restriction in GID/CTLH knockout BMDM[h]s. We first checked the levels of GABA signaling in mutant macrophages by staining the cells for total endogenous GABA with an anti-GABA antibody. Murine BMDMs and lung macrophages express functional GABA in resting states[53], and we assessed levels of GABA in uninfected scramble BMDM[h]s by confocal microscopy (Fig. S10A). All the three uninfected GID/CTLH knockout BMDM[h]s had significantly higher levels of GABA as compared to scramble sgRNA (Figs. S10A and 6B). It was previously shown that *Mtb* infection of mouse BMDMs in vitro and in vivo significantly decreases GABA levels[53]. In agreement with these findings, we observed a marked reduction of GABA expression in *Mtb*-infected scramble BMDM[h]s (Fig. 6A). In contrast, *Mtb* infection significantly amplified GABA levels in GID/CTLH knockout BMDM[h]s to even greater levels than uninfected cells (Fig. 6A, B).

Increased GABAergic signaling can positively modulate intracellular Ca²⁺ mobilization[68]. Moreover, Ca²⁺ signaling and transport were over-represented in GID/CTLH knockout BMDM[h]s commonly upregulated genes (Fig. 4D). We, therefore, checked intracellular Ca²⁺ mobilization in GID/CTLH knockout BMDM[h]s by loading the cells with a cell-permeable fluorogenic calcium-binding dye (Fluoforte®) followed by quantification of emitted fluorescence post stimulation with a Ca²⁺ mobilization agonist, adenosine triphosphate (ATP). Compared to scramble sgRNA BMDM[h]s, uninfected GID/CTLH knockout BMDM[h]s displayed increased intracellular calcium mobilization as evidenced by significantly higher normalized fluorescence 5 minutes after stimulation with ATP (Fig. S10B). In common with GABA signaling, *Mtb* infection significantly reduced Ca²⁺ mobilization in scramble BMDM[h]s but amplified the responses in GID/CTLH knockout macrophages (Fig. S10B). These functional data corroborate our host dual RNA-seq data sets, which showed a specific enrichment of GABAergic and Ca²⁺ signaling pathways in *Mtb*-infected GID/CTLH knockout macrophages (Fig. 4D, Supplementary Data 5).

GID/CTLH knockout macrophages are more autophagic and anti-inflammatory

Increased GABA signaling in macrophages enhances anti-microbial responses by promoting autophagy[53]. GABARAPL1, one of the upregulated GABA type A receptor in GID/CTLH knockout BMDM[h]s (Supplementary Data 4) is a homolog of the autophagy related protein 8 (*ATG8*)[69]. Genes involved in the autophagic process (*ATG9B, TRIM2, TRIM7,* and *TRIM16)* were also among the most significantly upregulated in *Mtb* infected GID/CTLH knockout BMDM[h]s (Supplementary Data 4). Moreover, in both uninfected and *Mtb* infected conditions, GID/CTLH knockout BMDM[h]s display significantly increased AMPK phosphorylation (Figs. 3E–G and S8A, B). AMPK activates catabolic processes like autophagy as part of the energy stress response in cell-starvation conditions[46]. These observations suggested that GID/CTLH knockout BMDM[h]s may be more autophagic as part of their anti-microbial responses. We therefore checked autophagic flux in GID/CTLH knockout BMDM[h]s by (1) immunoblotting to monitor the
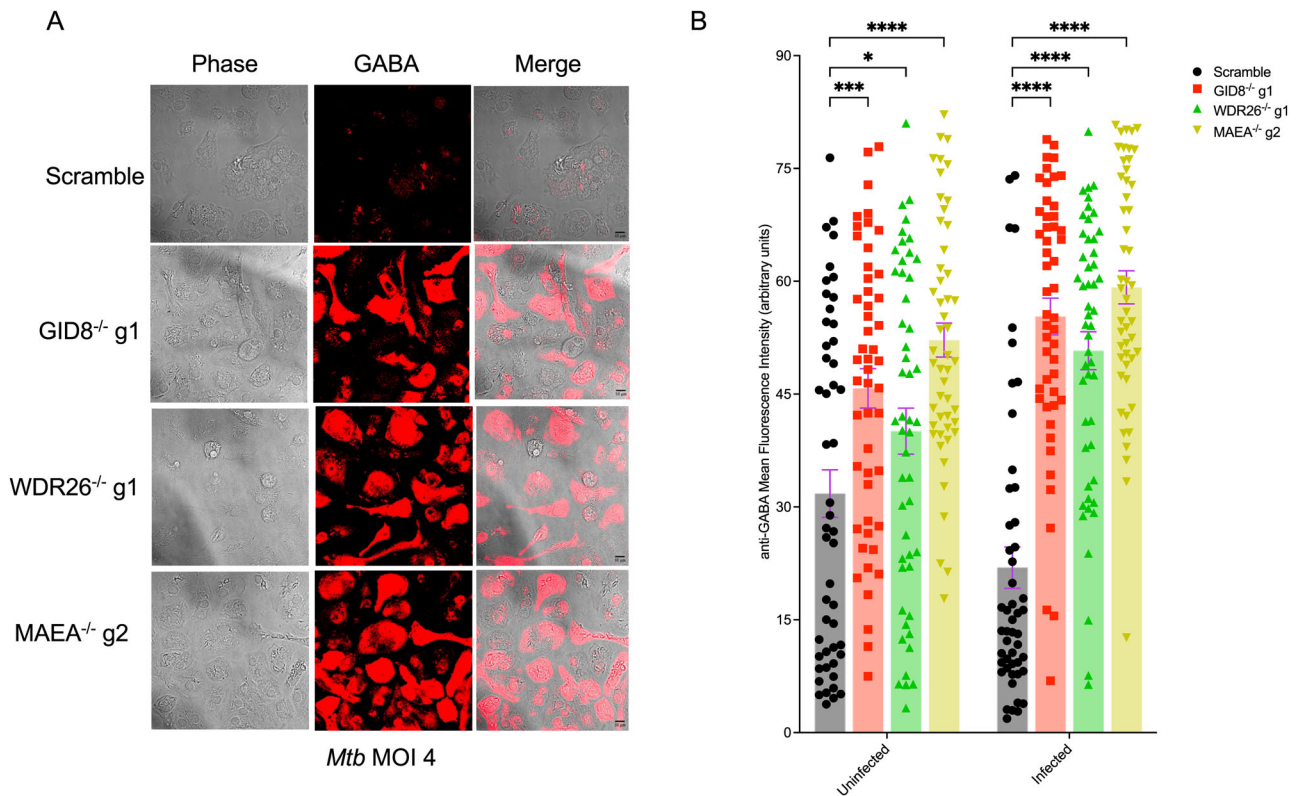
Fig. 6 | Increased GABAergic signaling in *Mtb* infected GID/CTLH knockout macrophages. A Representative confocal images of *Mtb* infected anti-GABA stained BMDM^{h}s. Scramble, *GID8$^{-/-}$*, *MAEA$^{-/-}$* and *WDR26$^{-/-}$* BMDM^{h}s were infected with the *Mtb* Erdman hsp60::GFP strain at MOI 4 for 24 hours. Fixed and permeabilized cells were then stained with anti-GABA (red) for confocal imaging.

B Quantification of mean fluorescence intensities (MFI) of GABA staining in (**A**) and Fig. S10A. MFI was quantified in at least 50 cells for both scramble and knockouts; $n = 50$ cells. *$P < 0.05$; ***$P < 0.001$; ****$P < 0.0001$, two-way ANOVA alongside Dunnett's multiple comparison test. Data are presented as mean values ± SD. Source data are provided as a Source Data file.

turnover of the microtubule-associated protein light chain 3 (LC3) from its LC3I to LC3II version (2) confocal imaging of anti-LC3 stained cells to quantify total LC3 puncta per individual cell and LC3 colocalizing with fluorescent *Mtb*. We observed significantly increased autophagic flux in *Mtb* infected GID/CTLH knockout BMDM^{h}s as evidenced by high LC3I to LC3II turnover ratios when compared to scramble BMDM^{h}s (Figs. 7A, B, and S11A, B). The magnitude of LC3I to LC3II turnover proportionally increased based on the bacterial burden at different MOIs (Figs. 7A, B and S11A, B). Some GID/CTLH knockout BMDM^{h}s (*MAEA$^{-/-}$*) displayed increased LC3I to LC3II turnover even in uninfected conditions (Figs. 7A, B, and S11A, B). Furthermore, *Mtb*-infected GID/CTLH knockout BMDM^{h}s displayed significantly higher numbers of total LC3 puncta per cell as compared to scramble when we analyzed the anti-LC3 stained cells by confocal microscopy (Fig. S11C, D). More importantly, GFP expressing *Mtb* significantly colocalized with LC3 in GID/CTLH knockout BMDM^{h}s (Fig. S11C, E) when compared to scramble sgRNA, which indicated increased autophagic targeting of *Mtb* in these mutant macrophages. Even though knockout of the GID/CTLH member, *MAEA*, has been shown to impair autophagy[70] in hematopoietic stem cells, our data supports the contention that increased autophagy is one of the main drivers of *Mtb* restriction in GID/CTLH knockout macrophages.

Mtb infected macrophages with increased GABA expression also diminish the expression of pro-inflammatory markers[53]. We checked the expression of pro-inflammatory markers (IL-1β and type 1 interferons (IFN-β)) in GID/CTLH knockout macrophages during the early stages of *Mtb* infection. We already observed a significant downregulation of pro-inflammatory markers including Tnf and IL-1β in GID/CTLH knockout macrophages in our RNA-seq data, collected 4 days post infection (Fig. S9). We concentrated our further analysis

of the expression of IFN-β and IL-1β in the first 24 hours of infection. qPCR analysis showed that *Mtb* infection caused a significant upregulation of IFN-β mRNA in scramble macrophages 4 hours post infection, but this response diminished 24 hours post infection (Fig. 7C). In contrast, IFN-β mRNA expression was completely suppressed in GID/CTLH knockout macrophages at both time points, and this was confirmed by ELISA quantification of IFN-β in cell supernatants 24 hours post infection (Fig. 7C). mRNA levels of IL-1β significantly increased in GID/CTLH knockout macrophages during the early 4 hours of infection, but this quickly resolved after 24 hours of infection to non-significant levels (Fig. S12A). This contrasted with depleted levels of IL-1β mRNA 4 days post infection in our RNA-seq data (Fig. S9B, C). We were, however, able to confirm by ELISA that the reduction of IL-1β mRNA expression at 24 hours corresponds with significantly lower levels of released IL-1β in culture supernatants as compared to scramble sgRNA (Fig. S12A). Western blot analysis demonstrated that both the pro and mature versions of IL-1β were equally impacted (Fig. S12B), suggesting that the anti-IL-1β properties of GID/CTLH knockout could be occurring upstream of IL-1β caspase mediated processing. These data provide further evidence that GID/CTLH knockout impairs the production of pro-inflammatory markers in *Mtb*-infected macrophages.

Discussion

In this report, we have employed a high throughput CRISPR genetic screen in primary macrophages to identify host effectors which, upon perturbation, improve the control of intracellular replication of *Mtb*. In the screen, pathways known previously to interfere with *Mtb* growth when perturbed, such as mTOR signaling and the mitochondrial OXPHOs, were specifically enriched. However, we also identified a
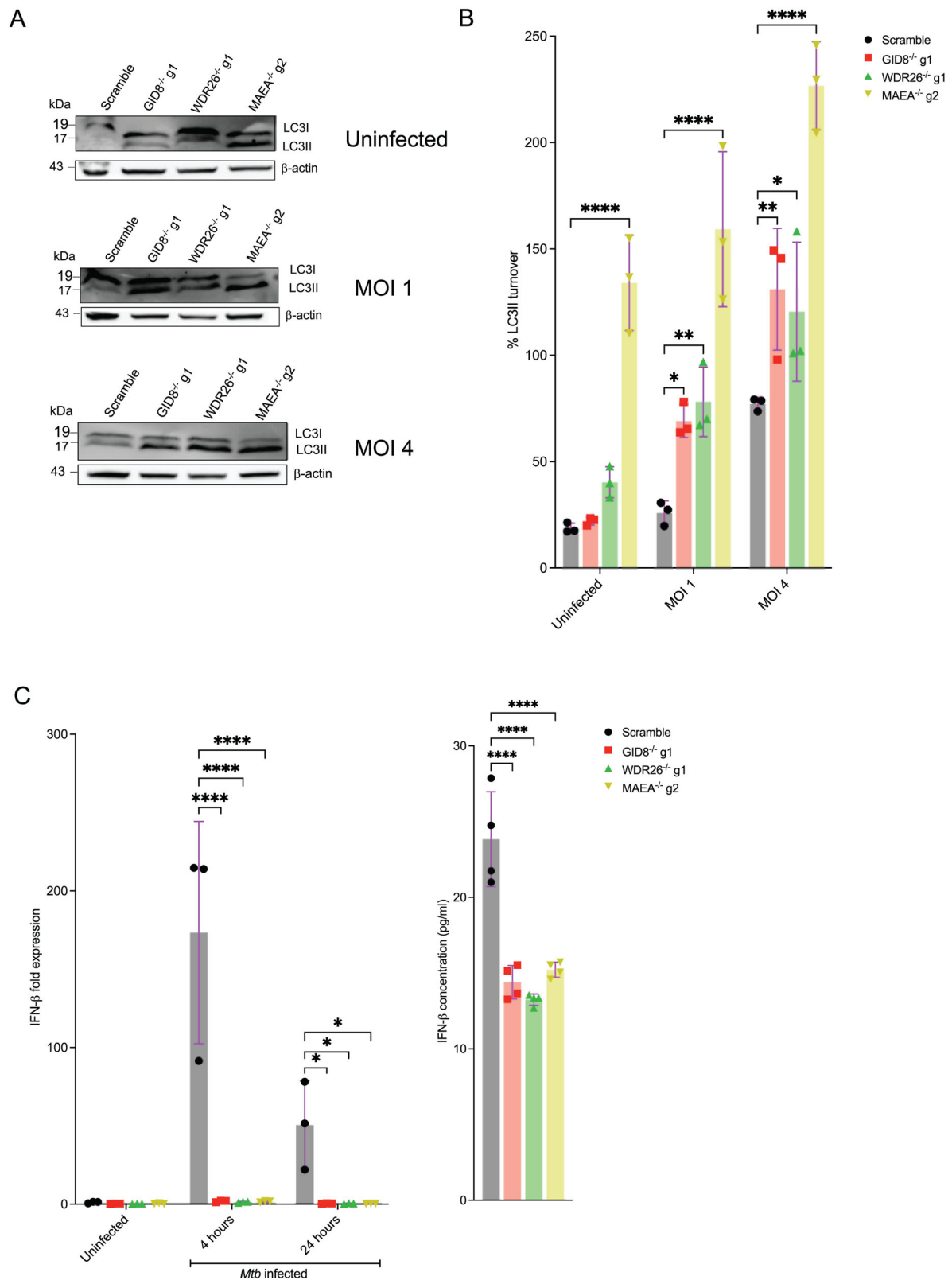
Fig. 7 | *Mtb* infected GID/CTLH knockout macrophages are more autophagic and anti-inflammatory. A Western blot analysis of autophagic LC3I to LC3II turnover in uninfected and *Mtb* infected scramble or *GID8⁻/⁻*, *MAEA⁻/⁻*, and *WDR26⁻/⁻* BMDMʰs at indicated MOIs. **B** Densitometry quantification (in %) of LC3I to LC3II turnover (LC3II/LC3I ratio) in (**A**) and Fig. S11A, B as normalized to β-actin; $n = 3$ biological replicates. *$P < 0.05$; **$P < 0.01$; ****$P < 0.0001$, two-way ANOVA alongside Dunnett's multiple comparison test. Data are presented as mean values ± SD. **C** Analysis of the expression of interferon 1 beta (IFN-β) in scramble or *GID8⁻/⁻*,

MAEA⁻/⁻ and *WDR26⁻/⁻ Mtb* infected macrophages. BMDMʰs were infected at MOI 4, and RNA was extracted for qPCR at 4 and 24 hours post infection; $n = 3$ biological replicates. *$P < 0.05$; ****$P < 0.0001$, two-way ANOVA alongside Dunnett's multiple comparison test. Data are presented as mean values ± SD. ELISA was carried out in culture supernatants 24 hours post infection; $n = 4$ biological replicates. ****$P < 0.0001$, one-way ANOVA alongside Dunnett's multiple comparison test. Data are presented as mean values ± SD. Source data are provided as a Source Data file.

novel role for the mammalian GID/CTLH complex in macrophage anti-microbial properties and found that its presence and activity correlated inversely with intracellular *Mtb* replication.

The GID/CTLH complex is an evolutionarily conserved member of the E3 ubiquitin-proteasome system, which was initially identified in yeast as a regulator of gluconeogenesis[32] but is more functionally diverse in higher eukaryotes[34]. With up to 12 functional members of the complex identified in mice and humans[30,34], the catalytic core of the complex is formed by the 2 RING proteins MAEA and RMND5A, while GID8 (TWA1) is a predicted scaffold that holds the complex together[30]. The biological significance of the complex in mammals is still being investigated[34]. However, it is ubiquitously expressed in most mammalian cells[30], which suggests its activities may have evolved to fulfill diverse functions. As we show in this study, all 12 members of the GID/CTLH complex appear to be actively transcribed in macrophages. Individual knockout of >50% of the GID/CTLH complex members in murine and human macrophages renders these phagocytes hostile to the intracellular replication of both *Mtb* and *S*. Typhimurium. It has been suggested that the GID/CTLH complex is involved in regulating cell proliferation, death, and survival pathways[34]. SiRNA-mediated knockdown of the GID/CTLH complex member RANBP9 made the cells more resistant to programmed cell death[71,72]. Indeed, knockout of the GID/CTLH complex in macrophages also rendered these phagocytes more resistant to *Mtb* induced necrotic cell death, a favorable host outcome, which can limit bacterial spread and virulence[11,14]. Moreover, GID/CTLH knockout in macrophages reprogrammed these cells to a more glycolytic state with increased activation of AMPK in line with previous observations[41,42]. Our results also identified additional anti-microbial responses upregulated in GID/CTLH complex knockout macrophages, such as the NADPH oxidase, autophagy, GPCR signaling, iron efflux, GABAergic signaling, and intracellular Ca^{2+} mobilization. GABAergic signaling has only recently been implicated in macrophage control of intracellular bacterial pathogens by promoting autophagy and inhibiting the production of pro-inflammatory cytokines[53]. Our results independently corroborate these findings as we observe increased GABA levels in GID/CTLH knockout BMDM^{h}s, which is accompanied by enhanced autophagy and elevated anti-inflammatory properties. Dual RNA-seq also revealed that *Mtb* residing in GID/CTLH knockout macrophages displayed transcriptional signatures consistent with nutritional stress as characterized by the upregulation of iron scavenger pathways, cholesterol breakdown, amino acid metabolism, fatty acid import, and oxidation.

There is an increased interest in the incorporation of HDTs in anti-TB drug regimens as a possible means of shortening the duration of treatment[28,51,73,74]. In theory, HDTs have the potential to (1) enhance host immune responses (2) promote macrophage control of intracellular *Mtb* (3) reduce non-productive and tissue injurious inflammation to improve lung function, and (4) minimize host stresses that lead to induction of *Mtb* drug tolerance[74]. As we report, knockout of the GID/CTLH complex in macrophages induces a broad range of anti-TB responses and results in anti-inflammatory host cells, which suggests it would make a tractable target for HDTs against *Mtb*. Several members of this complex are upregulated in a variety of cancers, and targeting this complex for cancer therapeutics is an area of current interest[34,75–77]. As efforts continue to identify novel HDTs against TB[1,51,74,78], the GID/CTLH complex offers an attractive target, and discovery efforts could benefit from the emerging therapeutic pursuit of the complex in the cancer field.

Methods

Ethics statement
The protocols used in this study have been reviewed and approved by the Institutional Biosafety Committee (protocol #16291-3) and the Institutional Animal Care and Use Committee (protocol # 2011-0086) at Cornell University.

Bacterial strains
The parent *Mtb* Erdman *strain* (ATCC 35801, PDIM positive) was used in all CFU experiments. Fluorescent *Mtb* reporters in the Erdman background; *Mtb* Erdman smyc'::mCherry and *Mtb* Erdman hsp60::GFP have been described previously[79,80]. The *Mtb* Erdman-Lux strain was generated by transformation with the pMV306G13+Lux plasmid[81]. *Mtb* was grown to log phase at 37 °C in MiddleBrook 7H9 broth supplemented with 10% oleic acid/albumin/dextrose/catalase (OADC Enrichment; Becton, Dickinson and Company), 0.2% glycerol, and 0.05% tyloxapol (Sigma-Aldrich). Reporter strains were maintained in the presence of an appropriate antibiotic; *Mtb* Erdman-Lux *Mtb* strain: 25 μg/ml kanamycin, *Mtb* Erdman hsp60::GFP: 25 μg/ml kanamycin and 50 μg/ml hygromycin, *Mtb* Erdman smyc'::mCherry: 50 μg/ml hygromycin. For *Salmonella* experiments, wild-type *S*. Typhimurium (CA32; ATCC 14028s) and the BFP expression strain *S*. Typhimurium CA4705 phoN::BFP[39] were used. *Salmonella* strains were propagated at 37 °C in Luria-Bertani (LB) broth.

Mammalian cells and culture
Murine Hoxb8-Estradiol (ER) responsive Cas9$^+$ eGFP conditionally immortalized myeloid progenitor cells were generated as previously described[22]. Hoxb8-ER cells were maintained in RPMI (Corning®) supplemented with 10% fetal bovine serum (FBS), 2 mM L-glutamine, 1 mM sodium pyruvate, 20 ng/ml murine GM-CSF (PeproTech), 0.5 μM β-estradiol, 10 mM HEPEs and 1% penicillin/streptomycin. To obtain BMDM^{h}s from Hoxb8-ER myeloid progenitors, cells were rinsed twice with 1× PBS to completely remove β-estradiol and resuspended in BMDM differentiation media; DMEM (Corning®) supplemented with 10% FBS, 15% L-cell conditioned media, 2 mM L-glutamine, 1 mM sodium pyruvate, and 1% penicillin/streptomycin at 37 °C for 6–7 days. Cells were maintained at a density of ~0.5 × 10^6 cells/ml during differentiation. The HEK-293FT cell line was purchased from Invitrogen and cultured in DMEM supplemented with 10% FBS, 1% non-essential amino acids, 2 mM L-glutamine, 1 mM sodium pyruvate, and 1% penicillin/streptomycin. Human monocytes were commercially obtained from the University of Nebraska Medical Center Elutriation Core and differentiated to HMDMs in DMEM medium with 2 mM L-glutamine, 1 mM sodium pyruvate, 10 mM HEPES, 1% penicillin/streptomycin and 10% pooled human serum (Sera Care).

Infection of macrophages with *Mtb*
BMDM^{h}s were infected with *Mtb* as previously described[82]. Briefly, log phase bacteria were pelleted, resuspended in basal uptake buffer (25 mM dextrose, 0.5% bovine serum albumin, 0.1% gelatin, 1 mM $CaCl_2$, 0.5 mM $MgCl_2$ in PBS) and syringed with a tuberculin syringe for at least 20 times. Bacteria were then resuspended in antibiotic free macrophage media before infection at specified MOIs.

CFU quantification of intracellular bacteria
Confluent macrophage monolayers (human and murine) were infected with *Mtb* at an appropriate MOI. After 3–4 hours, extracellular bacteria were removed by washing with fresh macrophage media at least three times. At indicated time points, macrophages were lysed with 0.01% SDS in water for 15 minutes and serially diluted in 0.05% Tween-80 in 1× PBS. Lysates were plated on 7H10 OADC agar plates and incubated at 37 °C for CFU counting 3–4 weeks later.

Cloning of sgRNAs, lentiviral production, and transduction
sgRNAs for CRISPR-mediated gene knockouts (Supplementary Data 3) were selected from the Brie murine knockout library[23] or ordered in predesigned form from IDT for human CRISPR RNP targets. For lentiviral delivery of sgRNAs, oligo pairs were annealed and cloned into the pLentiGuide-Puro (Addgene #52963). sgRNA inserts were confirmed by sequencing. To generate lentivirus particles for transduction, pLentiGuide-Puro plasmids with sgRNAs of interest were co-

transfected with Invitrogen packaging plasmids (pLP1, pLP2, and pLP/VSVG) in 293FT cells using the Lipofectamine 3000 lentiviral production protocol according to manufacturer's guidelines. To transduce Hoxb8 Cas9+ eGFP progenitors, 2.5×10^5 cells in 12-well plates were spin-infected at $1000 \times g$ for 90 minutes at 32 °C in the presence of 10 µg/ml protamine sulfate. 48 hours post-transduction, 8 µg/ml puromycin was added and maintained for 4 days. After the 4-day selection period, puromycin-resistant cells were briefly expanded for 1–2 days and frozen for future experiments. To quantify CRISPR editing efficiencies, total genomic DNA was prepared from cell pellets using the Qiagen DNeasy Blood and Tissue kit from which genomic sites surrounding the sgRNA target sites were PCR amplified using the Invitrogen Platinum *Taq* polymerase. Population-level editing efficiencies were estimated using ICE[37] and western blot analysis of differentiated BMDM^h s.

CRISPR screen knockout library preparation
The murine Brie knockout library was obtained from Addgene (#73633)[23]. The library (in pLentiGuide-Puro background) contains 78,637 sgRNAs targeting 19,674 genes (four sgRNAs/gene) with an additional 1000 non-targeting sgRNA controls. The library was amplified using the Moffat's lab CRISPR knockout library amplification protocol[83]. To generate lentivirus, 293FT cells were transfected as described above, scaling up tissue culture flasks depending on the amount of virus required to achieve desired library coverage. ~180 million Cas9 eGFP Hoxb8 progenitor cells were then transduced with the lentiviral library in the presence of 8 µg/ml polybrene at an MOI of ~0.3 (8 12-well plates, 2×10^6 cells/well, >700× library coverage) to ensure that only a single gene was targeted in every cell. 48 hours post-transduction, cells were selected with 8 µg/ml puromycin for 4 days and frozen in multiple aliquots of >40 million cells (>500× library coverage). Before screening, each aliquot was thawed and allowed to recover in Hoxb8 media for 3–4 days. Cells were then rinsed in 1× PBS at least 2 times before transfer into BMDM differentiation media to generate BMDM^h s knockout libraries.

Mtb infection of BMDM^h knockout library, antibody staining, and flow sorting
The BMDM^h knockout library was infected with the *Mtb* Erdman strain at MOI 1 for 4 days. The screen was carried out in three independent replicates with ~200 million cells per replicate (2 T-300 flasks). On day 4, all the cells were harvested by initially pretreating cell monolayers with Accutase for 5–10 minutes at room temperature, followed by scrapping in cold 1× PBS. Harvested cells were stained with the live/dead viability dye eFlour 506 (Invitrogen; 1:1000) and the PE anti-mouse/human CD11b antibody (Biolegend; 1:500) for 30 minutes at 4 °C. Stained cells were fixed in paraformaldehyde (PFA) for >1 hour before FACS of cells in the live gate. FACS was carried out on a Sony MA900 sorter, and a minimum of 10 million cells were sorted per replicate to achieve a >150× library coverage.

DNA extraction, barcode amplification, sequencing and analysis
Genomic DNA was extracted from the sorted cells as well as the unperturbed input library at full coverage (>300× library coverage) using a modified salt precipitation protocol as described previously[84]. Briefly, for $3 \times 10^7 – 5 \times 10^7$ frozen cell pellets (scaled down proportionally for lower cell numbers), 6 ml of NK Lysis Buffer (50 mM Tris, 50 mM EDTA, 1% SDS, pH 8) and 30 µl of 20 mg/ml Proteinase K (Qiagen) were added to the cells in a 15 ml falcon tube and incubated at 55 °C overnight to lyse the cells and de-crosslink PFA fixation. Next day, 30 µl of 10 mg/ml RNAse A diluted in NK lysis buffer was added to the lysed sample and incubated at 37 °C for 30 minutes. Samples were chilled on ice before the addition of 7.5 mM ice-cold ammonium acetate to precipitate proteins. After a brief vortex, insoluble protein fractions were pelleted by

centrifugation at $\geq 4000 \times g$ for 10 minutes. The supernatant was transferred to a new 15 ml falcon tube and DNA was precipitated with Isopropanol. Precipitated DNA was washed three times with 70% ethanol and airdried. Dried pellets were dissolved in sterile nuclease-free water and DNA concentration was measured on a Nanodrop 1000 (Thermo Scientific). Amplification of sgRNAs cassettes from the extracted DNA was performed using Illumina compatible primers from IDT as described previously[23] with some minor modifications. PCR amplification was carried out using KAPA HIFI Hotstart PCR (Roche) with the following reaction mixture in a 50 µl volume: 10 µL 5× reaction buffer, 1.5 µL dNTP, 1.5 µL P5 primer mix, 10 µM, 1.5 µL of P7 primer 10 µM, 2.5 µl DMSO, 0.5 µL polymerase, up to 2 µg of genomic DNA or 10 ng of plasmid DNA, up to 50 µL with water. PCR cycling conditions were as per manufactures protocol. Target PCR products were gel extracted using the Qiagen gel extraction kit and re-purified with the GeneJET PCR Purification kit (Thermo) before sequencing on an Illumina NextSeq500. Fastq files were mapped to the sgRNA library Index using MAGeCK-VISPR v0.5.6, which allows for automated trimming of adaptors and identification of sgRNA length[24]. Ranked sgRNA and gene hits were similarly obtained with the MAGeCK-VISPR workflow using Robust Rank Aggregation.

GO term enrichment
GO term enrichment was carried out in R using the enrichGO function of clusterProfiler v4.12.2[49]. Enriched BP, CC, or MF were filtered based on an adjusted *p* value of <0.05. In some cases, top enriched terms were visualized by tree plots of related GO clusters

Seahorse flux analyses
Extracellular flux analyses to measure OCRs and ECARs were performed using the Seahorse-8 XFp flux analyzer (Agilent). BMDM^h s were plated at a density of 1×10^5 cells/well in eight-well Seahorse plates overnight. Cells were then infected with *Mtb* Erdman strain at MOI 1 or left uninfected for another 24 hours. 1 hour before the assay, BMDM^h media was replaced with Seahorse base medium (without phenol red and sodium bicarbonate, with 5 mM HEPES) and placed at 37 °C in a non-CO$_2$ incubator. For the Mito stress test to measure OCR, 10 mM glucose, 2 mM L-glutamine, and 1 mM sodium pyruvate were added to the Seahorse base medium, while only glutamine was added for the Glycolysis stress test to measure ECARs. OCR and ECAR measurements (normalized to the number of seeded cells per well) were performed in line with specific kit instructions by sequential injection of oligomycin (2.5 µM), FCCP, fluoro-carbonyl cyanide phenylhydrazone (1.5 µM), rotenone/antimycin A (0.5 µM) for the Mito stress assay and glucose (10 mM), oligomycin (2.5 µM), 2-Deoxy-D-glucose (50 mM) for the Glycolysis stress assay. Three measurements were taken under basal conditions and after each drug injection.

Western blot analysis
Cells were washed in ice-cold 1× PBS and lysed with RIPA buffer (Thermo Fisher) containing protease inhibitors (Roche) for 30 minutes at 4 °C with gentle agitation. The Pierce™ Rapid Gold BCA Protein Assay Kit (Thermo Fisher) was used to measure the concentration of protein lysates. Equal amounts of protein (30 µg) were separated by SDS PAGE on a 4–20% gradient gel and transferred to a nitrocellulose membrane. The membrane was blocked for non-specific binding by incubating with 5% non-fat milk in PBST (0.1% tween in 1× PBS) for at least 30 minutes. Blots were washed and incubated with primary antibodies diluted in 2% non-fat milk in PBST at 4 °C overnight. The following primary antibodies were used in western blot analyses. Anti-AMPKα Mab (1:1000, Cell signaling Technology), anti-Phospho-AMPKα Mab (1:500, Cell signaling Technology), anti-β Actin (1:1000, Cell Signaling Technology), anti-LC3B (1:1000, Cell Signaling Technology), anti-GID8 (1:1000, Proteintech), anti-YPEL5 (1:1000, Proteintech), anti-WDR26 (1:300, Bioss), anti-UBE2H (1:1000,

Proteintech), anti-MAEA (1 μg/ml, R&D Systems), anti-MKLN1 (1:250, Proteintech), anti-RANBP9 (1:1000, Proteintech) anti-IL-1β (1:1000, Cell Signaling Technology). Secondary antibodies used were horseradish peroxidase-conjugated polyclonal donkey anti-sheep IgG (1:1000, R&D Systems) and anti-rabbit/mouse StarBright Blue 700 (1:2500, Biorad). Blots were developed by the SuperSignal™ West Atto Ultimate Sensitivity Substrate (Thermo Fisher) or directly imaged in case of fluorescent secondary antibodies. Images were acquired on a ChemiDoc MP imaging system (Biorad). Western blot band intensities were quantified in ImageJ.

Dual RNA-sequencing of BMDM^h *Mtb* infected macrophages
Dual RNA-sequencing of *Mtb* infected BMDM^{h}s was carried out as described previously[47,85] with modifications as described below. Briefly, BMDM^{h}s were infected with the *Mtb* Erdman smyc'::mCherry reporter strain at MOI 0.5. Four days post infection, cells were harvested and stained with the live/dead viability dye eFlour 506 (Invitrogen; 1:1000) and the PE anti-mouse/human CD11b antibody (Biolegend; 1:500) for 30 minutes at 4 °C. Live mCherry Cd11b positive cells were sorted on a Sony MA900 sorter. 250,000 *Mtb* infected sorted macrophages were spun down, resuspended in 150 μl sorter buffer, and transferred to a tube containing 600 μl Trizol. Samples were mixed and incubated at room temperature for 5 minutes followed by centrifugation at -12,000 × g for 20 minutes to pellet the bacteria. 600 μl of Trizol supernatant (host RNA) was then transferred to a new tube. Fresh 400 μl of Trizol was added to the tube containing the bacterial pellet together with 150 μl of zirconia beads. Bead beating was performed on a FastPrep-24™ bead beater (MP biomedicals) in 2 cycles of 1 minute, resting 2 minutes on ice between each cycle. 40% of host RNA (-240 μl) was then added back to the original bead-containing tube, which allows for a good proportion capture of both host and bacteria transcripts by getting rid of some of the host RNA[47,85]. Chloroform was added (200 μL of chloroform for 1 mL of Trizol) to the tubes which were mixed thoroughly and spun at 12,000 × g for 15 minutes at 4 °C. Total RNA was purified from the aqueous phase using the Zymo RNA clean and concentrator-5 kit according to manufactures instructions. Ribosomal RNA (rRNA) depletion in the RNA samples was performed using the QIAseq FastSelect pan-bacterial and H/M/R kits in the duo-depletion mode. Libraries were prepared from rRNA-depleted samples using the NEBNext Ultra II Directional RNA Library Prep Kit (New England Biolabs) and sequenced on the Novaseq 6000 S4 (Illumina). Paired-end sequenced reads were mapped to the mouse reference genome (GRCm39) and the *Mtb* H37Rv genome (ASM19595v2) using STAR-2.7.10b. Raw counts were obtained using HTSeq v2.02 with GRCm39 and ASM19595v2 annotations. Normalization of read counts and differential expression analysis were performed in R using DESeq2 v1.44.0 and APEGLM v1.26.1 for log fold change estimation as described previously[47,85]. Genes with <10 raw counts were excluded from downstream analyzes. Pathway enrichment was performed on DE genes using clusterProfiler as described in the prior section.

Intracellular Ca^{2+} mobilization assay
BMDM^{h}s were seeded in 96-well black clear bottom plates at a density of 1×10^5 cells/well and incubated at 37 °C in 5% CO$_2$ overnight. The next day, macrophage media was discarded and replaced with the Fluoforte® dye (Enzo Life) in 100 μl Hank's balanced salt solution (HBSS) in the presence of a dye efflux inhibitor. After 1 hour of incubation (45 minutes at 37 °C and 15 minutes at room temperature), 20 μl of 6 μM ATP was added to each well for a final concentration of 1 μM. Fluoforte® fluorescence (excitation 490 nM/emission 525 nM) was quantified at time 0 (baseline) and after 5 minutes on an Envision plate reader (PerkinElmer). Normalized relative fluorescence units (ΔRFU) were calculated for each well using the following formula:

ΔRFU = (Fluorescence taken after 5 minutes of ATP stimulation −Baseline fluorescence taken at the start of the assay)/Baseline fluorescence taken at the start of the assay.

Immunofluorescence and confocal microscopy
Macrophage monolayers in Ibidi eight-well chambers were infected with *Mtb* at an appropriate MOI as described in prior sections. At specified time intervals, cells were fixed with 4% PFA for >1 hour and permeabilized with 0.2% Triton X-100 (Sigma-Aldrich) for 15 minutes. Permeabilized cells were blocked with 3% bovine serum albumin (BSA) for 1 hour and incubated with primary antibody diluted in 3% BSA at 4 °C overnight. Next day, cells were washed with 1× PBS three times and incubated with secondary antibodies for 1 hour at room temperature. Primary antibodies used were anti-GABA (1:400, Sigma-Aldrich) and anti-LC3B (1:1000, Cell Signaling Technology). The Alexa Fluor™ 647 goat anti-rabbit secondary antibody (1:500, Thermo Scientific) was used. After mounting, images were acquired using a Leica SP5 confocal microscope. Z-stacks were re-constructed in ImageJ, from which mean fluorescence intensities (MFI) for individual cells or colocalizations were performed.

CRISPR RNP delivery in human monocyte-derived macrophages
Isolated human monocytes were left in culture for 24 hours before transfection. On the day of transfection, cells were harvested, washed with 1× PBS, and resuspended in P3 Primary Cell Nucleofection Buffer (Lonza) at a concentration of 5×10^6 cells in 20 μl for each electroporation. Equal volumes of 100 μM Alt-R crRNA and Alt-tracrRNA (IDT) were annealed to form sgRNA duplexes by incubation at 95 °C for 5 minutes followed by cooling to room temperature for >15 minutes. To form CRISPR RNPs, annealed sgRNA duplexes were mixed with IDT Alt-R S.p. Cas9 Nuclease V3 at a 3:1 molar ratio and incubated for at least 20 minutes at room temperature. For nucleofection, 4 μl of CRISPR RNP was mixed with the 20 μl cell suspension in P3 buffer and transferred into the supplied nucleofector cassette strip. The strip was inserted into the Lonza 4D-Nucleofector and nucleofected with the Buffer P3, CM-137 conditions as previously described[40]. After nucleofection, cells were transferred into Petri dishes and allowed to complete differentiation to HMDMs for 5–6 days. Knockout efficiencies were confirmed in HMDMs by ICE analysis and western blot.

Quantitative RT-PCR
Total RNA was isolated from uninfected or *Mtb*-infected BMDM^{h}s using Trizol alongside the Zymo RNA clean and concentrator-5 kit according to manufactures' instructions. cDNA was synthesized from -1 μg of extracted RNA using an iScript cDNA synthesis kit (BioRad). RT-PCR was performed for IFN-β and IL-1β on the Applied Biosystems PRISM 7500 qPCR machine. Beta 2 microglobulin was used as a reference housekeeping gene. Predesigned qPCR primers were purchased from IDT. PCR reactions were carried out using iTaq Universal SYBR Green Supermix (BioRad).

ELISA
BMDM^{h}s in 96-well plates were infected with *Mtb* at an appropriate MOI for 24 hours. Cell culture supernatants were collected from infected cells and assayed for IFN-β and IL-1β using the IFN-β and IL-1β R&D ELISA kits according to manufactures' instructions.

General statistics
Basic statistical tests were carried out in GraphPad Prism 10. Comparisons between more than two groups were analyzed using one-way or two ANOVA alongside Dunnett's multiple comparison test. *P* values < 0.05 were considered statistically significant.

Reporting summary

Further information on research design is available in the Nature Portfolio Reporting Summary linked to this article.

Data availability

The dual RNA-seq data sets supporting the conclusions of this article are available in GEO: GSE267063. https://www.ncbi.nlm.nih.gov/geo/query/acc.cgi?acc=GSE267063. Source data of plotted graphs and uncropped versions of blots are provided as a Source Data file. Source data are provided with this paper.

References

1. WHO. Global tuberculosis report 2023. World Health Organisation, Geneva, Switzerland (2023).
2. Behr, M. A., Edelstein, P. H. & Ramakrishnan, L. Rethinking the burden of latent tuberculosis to reprioritize research. *Nat. Microbiol.* **9**, 1157–1158 (2024).
3. Sturgill-Koszycki, S. et al. Lack of acidification in *Mycobacterium phagosomes* produced by exclusion of the vesicular proton-ATPase. *Science* **263**, 678–681 (1994).
4. Upadhyay, S., Mittal, E. & Philips, J. A. Tuberculosis and the art of macrophage manipulation. *Pathog. Dis.* **76**, fty037 (2018).
5. Huang, L., Nazarova, E. V. & Russell, D. G. *Mycobacterium tuberculosis*: Bacterial fitness within the host macrophage. *Microbiol. Spectr.* **7**, 10.1128 (2019).
6. Russell, D. G. et al. *Mycobacterium tuberculosis* wears what it eats. *Cell Host Microbe* **8**, 68–76 (2010).
7. Wilburn, K. M., Fieweger, R. A. & VanderVen, B. C. Cholesterol and fatty acids grease the wheels of *Mycobacterium tuberculosis* pathogenesis. *Pathog. Dis.* **76**, fty021 (2018).
8. Guilliams, M. et al. Alveolar macrophages develop from fetal monocytes that differentiate into long-lived cells in the first week of life via GM-CSF. *J. Exp. Med.* **210**, 1977–1992 (2013).
9. Guilliams, M. & Scott, C. L. Does niche competition determine the origin of tissue-resident macrophages? *Nat. Rev. Immunol.* **17**, 451–460 (2017).
10. Huang, L., Nazarova, E. V., Tan, S., Liu, Y. & Russell, D. G. Growth of *Mycobacterium tuberculosis* in vivo segregates with host macrophage metabolism and ontogeny. *J. Exp. Med.* **215**, 1135–1152 (2018).
11. Behar, S. M. et al. Apoptosis is an innate defense function of macrophages against *Mycobacterium tuberculosis*. *Mucosal Immunol.* **4**, 279–287 (2011).
12. Martin, C. J. et al. Efferocytosis is an innate antibacterial mechanism. *Cell Host Microbe* **12**, 289–300 (2012).
13. Sun, J. et al. The tuberculosis necrotizing toxin kills macrophages by hydrolyzing NAD. *Nat. Struct. Mol. Biol.* **22**, 672–678 (2015).
14. Chen, M., Gan, H. & Remold, H. G. A mechanism of virulence: virulent *Mycobacterium tuberculosis* strain H37Rv, but not attenuated H37Ra, causes significant mitochondrial inner membrane disruption in macrophages leading to necrosis. *J. Immunol.* **176**, 3707–3716 (2006).
15. van der Wel, N. et al. *M. tuberculosis* and *M. leprae* translocate from the phagolysosome to the cytosol in myeloid cells. *Cell* **129**, 1287–1298 (2007).
16. Simeone, R. et al. Phagosomal rupture by *Mycobacterium tuberculosis* results in toxicity and host cell death. *PLoS Pathog.* **8**, e1002507 (2012).
17. Romagnoli, A. et al. ESX-1 dependent impairment of autophagic flux by *Mycobacterium tuberculosis* in human dendritic cells. *Autophagy* **8**, 1357–1370 (2012).
18. Shah, S. et al. Cutting edge: *Mycobacterium tuberculosis* but not nonvirulent *Mycobacteria* inhibits IFN-β and AIM2 inflammasome-dependent IL-1β production via its ESX-1 secretion system. *J. Immunol.* **191**, 3514–3518 (2013).
19. Zhang, L., Jiang, X., Pfau, D., Ling, Y. & Nathan, C. F. Type I interferon signaling mediates *Mycobacterium tuberculosis*-induced macrophage death. *J. Exp. Med.* **218**, e20200887 (2021).
20. Lai, Y. et al. Illuminating host-mycobacterial interactions with genome-wide CRISPR knockout and CRISPRi screens. *Cell Syst.* **11**, 239–251.e237 (2020).
21. Mahamed, D. et al. Intracellular growth of *Mycobacterium tuberculosis* after macrophage cell death leads to serial killing of host cells. *Elife* **6**, e22028 (2017).
22. Kiritsy, M. C. et al. Mitochondrial respiration contributes to the interferon gamma response in antigen-presenting cells. *Elife* **10**, e65109 (2021).
23. Doench, J. G. et al. Optimized sgRNA design to maximize activity and minimize off-target effects of CRISPR-Cas9. *Nat. Biotechnol.* **34**, 184–191 (2016).
24. Wang, B. et al. Integrative analysis of pooled CRISPR genetic screens using MAGeCKFlute. *Nat. Protoc.* **14**, 756–780 (2019).
25. Singh, P. & Subbian, S. Harnessing the mTOR pathway for tuberculosis treatment. *Front. Microbiol.* **9**, 70 (2018).
26. Kim, J. & Guan, K.-L. mTOR as a central hub of nutrient signalling and cell growth. *Nat. Cell Biol.* **21**, 63–71 (2019).
27. Gutierrez, M. G. et al. Autophagy is a defense mechanism inhibiting BCG and *Mycobacterium tuberculosis* survival in infected macrophages. *Cell* **119**, 753–766 (2004).
28. Singhal, A. et al. Metformin as adjunct antituberculosis therapy. *Sci. Transl. Med.* **6**, 263ra159 (2014).
29. Theriault, M. E. et al. Iron limitation in *M. tuberculosis* has broad impact on central carbon metabolism. *Commun. Biol.* **5**, 685 (2022).
30. Lampert, F. et al. The multi-subunit GID/CTLH E3 ubiquitin ligase promotes cell proliferation and targets the transcription factor Hbp1 for degradation. *eLife* **7**, e35528 (2018).
31. Kobayashi, N. et al. RanBPM, Muskelin, p48EMLP, p44CTLH, and the armadillo-repeat proteins ARMC8alpha and ARMC8beta are components of the CTLH complex. *Gene* **396**, 236–247 (2007).
32. Santt, O. et al. The yeast GID complex, a novel ubiquitin ligase (E3) involved in the regulation of carbohydrate metabolism. *Mol. Biol. Cell* **19**, 3323–3333 (2008).
33. Chen, S. J., Wu, X., Wadas, B., Oh, J. H. & Varshavsky, A. An N-end rule pathway that recognizes proline and destroys gluconeogenic enzymes. *Science* **355**, eaal3655 (2017).
34. Maitland, M. E. R., Lajoie, G. A., Shaw, G. S. & Schild-Poulter, C. Structural and functional insights into GID/CTLH E3 ligase complexes. *Int. J. Mol. Sci.* **23**, 5863 (2022).
35. Wang, L. et al. The Ran-binding protein RanBPM can depress the NF-κB pathway by interacting with TRAF6. *Mol. Cell Biochem.* **359**, 83–94 (2012).
36. Subramanian, M. et al. An AXL/LRP-1/RANBP9 complex mediates DC efferocytosis and antigen cross-presentation in vivo. *J. Clin. Invest.* **124**, 1296–1308 (2014).
37. Conant, D. et al. Inference of CRISPR edits from Sanger trace data. *CRISPR J.* **5**, 123–130 (2022).
38. Wu, J. et al. High-throughput assay to phenotype *Salmonella enterica* Typhimurium association, invasion, and replication in macrophages. *J. Vis. Exp.* e51759 (2014).
39. Eade, C. R. et al. *Salmonella* pathogenicity Island 1 Is expressed in the chicken intestine and promotes bacterial proliferation. *Infect. Immun.* **87**, e00503–e00518 (2019).
40. Freund, E. C. et al. Efficient gene knockout in primary human and murine myeloid cells by non-viral delivery of CRISPR-Cas9. *J. Exp. Med.* **217**, e20191692 (2020).
41. Maitland, M. E. R., Kuljanin, M., Wang, X., Lajoie, G. A. & Schild-Poulter, C. Proteomic analysis of ubiquitination substrates reveals a CTLH E3 ligase complex-dependent regulation of glycolysis. *FASEB J.* **35**, e21825 (2021).

42. Liu, H. et al. The GID ubiquitin ligase complex is a regulator of AMPK activity and organismal lifespan. *Autophagy* **16**, 1618–1634 (2020).

43. Shi, L., Jiang, Q., Bushkin, Y., Subbian, S. & Tyagi, S. Biphasic dynamics of macrophage immunometabolism during *Mycobacterium tuberculosis* infection. *mBio* **10**, e02550–18 (2019).

44. Gleeson, L. E. et al. Cutting edge: *Mycobacterium tuberculosis* induces aerobic glycolysis in human alveolar macrophages that is required for control of intracellular bacillary replication. *J. Immunol.* **196**, 2444–2449 (2016).

45. Cumming, B. M., Addicott, K. W., Adamson, J. H. & Steyn, A. J. *Mycobacterium tuberculosis* induces decelerated bioenergetic metabolism in human macrophages. *Elife* **7**, e39169 (2018).

46. Garcia, D. & Shaw, R. J. AMPK: mechanisms of cellular energy sensing and restoration of metabolic balance. *Mol. Cell* **66**, 789–800 (2017).

47. Pisu, D., Huang, L., Grenier, J. K. & Russell, D. G. Dual RNA-seq of Mtb-infected macrophages in vivo reveals ontologically distinct host-pathogen interactions. *Cell Rep.* **30**, 335–350.e334 (2020).

48. Donovan, A. et al. The iron exporter ferroportin/Slc40a1 is essential for iron homeostasis. *Cell Metab.* **1**, 191–200 (2005).

49. Wu, T. et al. clusterProfiler 4.0: a universal enrichment tool for interpreting omics data. *Innovation* **2**, 100141 (2021).

50. Malik, Z. A., Denning, G. M. & Kusner, D. J. Inhibition of Ca(2+) signaling by *Mycobacterium tuberculosis* is associated with reduced phagosome-lysosome fusion and increased survival within human macrophages. *J. Exp. Med.* **191**, 287–302 (2000).

51. Stanley, S. A. et al. Identification of host-targeted small molecules that restrict intracellular *Mycobacterium tuberculosis* growth. *PLoS Pathog.* **10**, e1003946 (2014).

52. Heisler, F. F. et al. Muskelin regulates actin filament- and microtubule-based GABA(A) receptor transport in neurons. *Neuron* **70**, 66–81 (2011).

53. Kim, J. K. et al. GABAergic signaling linked to autophagy enhances host protection against intracellular bacterial infections. *Nat. Commun.* **9**, 4184 (2018).

54. Krithika, R. et al. A genetic locus required for iron acquisition in *Mycobacterium tuberculosis*. *Proc. Natl Acad. Sci. USA* **103**, 2069–2074 (2006).

55. Pandey, S. D. et al. Iron-regulated protein HupB of *Mycobacterium tuberculosis* positively regulates siderophore biosynthesis and is essential for growth in macrophages. *J. Bacteriol.* **196**, 1853–1865 (2014).

56. Wipperman, M. F., Yang, M., Thomas, S. T. & Sampson, N. S. Shrinking the FadE proteome of *Mycobacterium tuberculosis*: insights into cholesterol metabolism through identification of an α2β2 heterotetrameric acyl coenzyme A dehydrogenase family. *J. Bacteriol.* **195**, 4331–4341 (2013).

57. Lack, N. A. et al. Characterization of a carbon-carbon hydrolase from *Mycobacterium tuberculosis* involved in cholesterol metabolism. *J. Biol. Chem.* **285**, 434–443 (2010).

58. Forrellad, M. A. et al. Role of the Mce1 transporter in the lipid homeostasis of *Mycobacterium tuberculosis*. *Tuberculosis* **94**, 170–177 (2014).

59. Nazarova, E. V. et al. Rv3723/LucA coordinates fatty acid and cholesterol uptake in *Mycobacterium tuberculosis*. *Elife* **6**, e26969 (2017).

60. Lott, J. S. The tryptophan biosynthetic pathway is essential for *Mycobacterium tuberculosis* to cause disease. *Biochem. Soc. Trans.* **48**, 2029–2037 (2020).

61. Zhang, Y. J. et al. Tryptophan biosynthesis protects *Mycobacteria* from CD4 T-cell-mediated killing. *Cell* **155**, 1296–1308 (2013).

62. Tews, I. et al. The structure of a pH-sensing Mycobacterial adenylyl cyclase holoenzyme. *Science* **308**, 1020–1023 (2005).

63. Bush, M. J. The actinobacterial WhiB-like (Wbl) family of transcription factors. *Mol. Microbiol.* **110**, 663–676 (2018).

64. Chen, Z. et al. Mycobacterial WhiB6 differentially regulates ESX-1 and the Dos regulon to modulate granuloma formation and virulence in Zebrafish. *Cell Rep.* **16**, 2512–2524 (2016).

65. Bosserman, R. E. et al. WhiB6 regulation of ESX-1 gene expression is controlled by a negative feedback loop in *Mycobacterium marinum*. *Proc. Natl. Acad. Sci. USA* **114**, E10772–e10781 (2017).

66. Kudhair, B. K. et al. Structure of a Wbl protein and implications for NO sensing by *M. tuberculosis*. *Nat. Commun.* **8**, 2280 (2017).

67. Khan, S. et al. Toxin-Antitoxin system of *Mycobacterium tuberculosis*: roles beyond stress sensor and growth regulator. *Tuberculosis (Edinb.)* **143**, 102395 (2023).

68. Levi, G. & Raiteri, M. Modulation of gamma-aminobutyric acid transport in nerve endings: role of extracellular gamma-aminobutyric acid and of cationic fluxes. *Proc. Natl Acad. Sci. USA* **75**, 2981–2985 (1978).

69. Weidberg, H. et al. LC3 and GATE-16/GABARAP subfamilies are both essential yet act differently in autophagosome biogenesis. *EMBO J.* **29**, 1792–1802 (2010).

70. Wei, Q. et al. MAEA is an E3 ubiquitin ligase promoting autophagy and maintenance of haematopoietic stem cells. *Nat. Commun.* **12**, 2522 (2021).

71. Atabakhsh, E., Bryce, D. M., Lefebvre, K. J. & Schild-Poulter, C. RanBPM has proapoptotic activities that regulate cell death pathways in response to DNA damage. *Mol. Cancer Res.* **7**, 1962–1972 (2009).

72. Liu, T., Roh, S. E., Woo, J. A., Ryu, H. & Kang, D. E. Cooperative role of RanBP9 and P73 in mitochondria-mediated apoptosis. *Cell Death Dis.* **4**, e476 (2013).

73. Hawn, T. R., Matheson, A. I., Maley, S. N. & Vandal, O. Host-directed therapeutics for tuberculosis: can we harness the host? *Microbiol. Mol. Biol. Rev.* **77**, 608–627 (2013).

74. Young, C., Walzl, G. & Du Plessis, N. Therapeutic host-directed strategies to improve outcome in tuberculosis. *Mucosal Immunol.* **13**, 190–204 (2020).

75. Ye, Y., Tang, X., Sun, Z. & Chen, S. Upregulated WDR26 serves as a scaffold to coordinate PI3K/ AKT pathway-driven breast cancer cell growth, migration, and invasion. *Oncotarget* **7**, 17854–17869 (2016).

76. Huffman, N., Palmieri, D. & Coppola, V. The CTLH complex in cancer cell plasticity. *J. Oncol.* **2019**, 4216750 (2019).

77. Jiang, G. et al. A novel biomarker ARMc8 promotes the malignant progression of ovarian cancer. *Hum. Pathol.* **46**, 1471–1479 (2015).

78. Dartois, V. A. & Rubin, E. J. Anti-tuberculosis treatment strategies and drug development: challenges and priorities. *Nat. Rev. Microbiol.* **20**, 685–701 (2022).

79. Sukumar, N., Tan, S., Aldridge, B. B. & Russell, D. G. Exploitation of *Mycobacterium tuberculosis* reporter strains to probe the impact of vaccination at sites of infection. *PLoS Pathog.* **10**, e1004394 (2014).

80. Dhandayuthapani, S. et al. Green fluorescent protein as a marker for gene expression and cell biology of Mycobacterial interactions with macrophages. *Mol. Microbiol.* **17**, 901–912 (1995).

81. Andreu, N. et al. Optimisation of bioluminescent reporters for use with *Mycobacteria*. *PLoS One* **5**, e10777 (2010).

82. Nazarova, E. V. & Russell, D. G. Growing and handling of *Mycobacterium tuberculosis* for macrophage infection assays. *Methods Mol. Biol.* **1519**, 325–331 (2017).

83. Hart, T. et al. Evaluation and design of genome-wide CRISPR/SpCas9 knockout screens. *G3 (Bethesda)* **7**, 2719–2727 (2017).

84. Chen, S. et al. Genome-wide CRISPR screen in a mouse model of tumor growth and metastasis. *Cell* **160**, 1246–1260 (2015).

85. Pisu, D., Huang, L., Rin Lee, B. N., Grenier, J. K. & Russell, D. G. Dual RNA-sequencing of *Mycobacterium tuberculosis*-infected cells from a murine infection model. *STAR Protoc.* **1**, 100123 (2020).

Acknowledgements

Author contributions

N.V.S. and D.G.R. conceptualized the study. L.J., P.P.B., and E.J contributed to the acquisition and analysis of data. C.A. and C.M.S. contributed to data interpretation. D.G.R. acquired funding for the study. N.V.S. and D.G.R. wrote the original draft. N.V.S., D.G.R., L.J., P.P.B., E.J., C.A., and C.M.S. reviewed and edited the manuscript.

Competing interests

The authors declare no competing interests.

Additional information

Supplementary information The online version contains supplementary material available at https://doi.org/10.1038/s41467-024-53637-z.

Correspondence and requests for materials should be addressed to David G. Russell.

Peer review information *Nature Communications* thanks Vincenzo Coppola, Laura Jenniches and the other, anonymous, reviewer(s) for their contribution to the peer review of this work. A peer review file is available.

Reprints and permissions information is available at http://www.nature.com/reprints

Publisher's note Springer Nature remains neutral with regard to jurisdictional claims in published maps and institutional affiliations.